Weakly nonlinear stability analysis of a flow past a neo-Hookean solid at arbitrary Reynolds numbers

Paresh Chokshi and V. Kumaran
Department of Chemical Engineering, Indian Institute of Science, Bangalore 560 012, India

(Received 15 August 2007; accepted 18 August 2008; published online 29 September 2008)

The finite amplitude stability of a plane Couette flow over a deformable solid medium is analyzed with emphasis on the class of high Reynolds number (Re) modes, referred to as the wall modes, for which the viscous stresses are confined to a thin layer adjacent to the fluid-solid interface with thickness $O(\mathrm{Re}^{-1/3})$ times the channel width in the limit $\mathrm{Re} \gg 1$. Here, the Reynolds number is defined in terms of the top plate velocity V and the channel width R. Previous linear stability analyses have shown that the wall modes are unstable for Newtonian flow past a linear viscoelastic solid. In the present study, the analysis is extended to examine the weakly nonlinear stability of these unstable wall modes in order to determine the nature of bifurcation of the transition point to finite amplitude states. To account for the finite strain deformations, the flexible solid medium is described by a neo-Hookean elastic model which is a generalization of the commonly used linear constitutive model. The linear stability analysis provides the critical shear rate Γ_c and the critical wavenumber in the axial direction α_c, where the dimensionless shear rate is defined as $\Gamma = \sqrt{\rho V^2 / G}$, where ρ is the fluid density and G is the shear modulus of the elastic solid. The critical parameter Γ_c for the neo-Hookean solid is found to be close to Γ_c for the linear elastic solid analyzed in the previous studies. The first Landau constant $s^{(1)}$, which is the finite amplitude correction to the linear growth rate, is evaluated in the weakly nonlinear stability analysis using both the numerical technique and the high Re asymptotic analysis. The real part of the Landau constant, $s_r^{(1)}$, is negative for the wall mode instability in the limit $\mathrm{Re} \gg 1$ for a wide range of dimensionless solid thickness H, indicating that there is a supercritical bifurcation of the wall mode instability. The amplitude of the supercritically bifurcated equilibrium state is derived in the vicinity of the critical point. The equilibrium amplitude, in the form $A_{1e}^2/(\Gamma - \Gamma_c)$, is found to scale as $\mathrm{Re}^{-1/3}$ in the limit $\mathrm{Re} \gg 1$ and is proportional to $H^{2.3}$ for $H \gg 1$ in the same limit. © *2008 American Institute of Physics*.
[DOI: 10.1063/1.2982521]

I. INTRODUCTION

The loss of stability of a laminar profile by the inertial forces has been studied extensively to comprehend the underlying mechanism of laminar-turbulent transition. At high Reynolds numbers, the asymptotic analyses of Corcos and Sellars[1] and Gill[2] for axisymmetric disturbances revealed that there exist two distinct classes of modes in a rigid pipe flow, namely, the *center modes* and the *wall modes*. Linear stability studies[3] indicate that both these modes are stable, though it has been speculated that these modes may be unstable to finite amplitude disturbances. In channels and tubes lined with flexible medium, it is well known that, due to their proximity with the solid boundary, the wall modes are affected by wall flexibility, and they could become unstable even to infinitesimally small disturbances.

In addition to the onset of transition, the wall mode instability may also be of relevance to the drag reduction in the turbulent flow past compliant surfaces. It is widely believed that the turbulence in a wall-bounded shear flow attains self-sustenance by the presence of mutually regenerating low-speed streaks with streamwise velocity and streamwise vortices.[4–6] These structures are a result of the "bursting" phenomenon in the near wall region with thickness around 50 wall units, and this bursting phenomenon is responsible for the production of most of the turbulent kinetic energy.[7] Wall mode disturbances confined to a thin layer near the wall may influence the bursting mechanism, thereby affecting the turbulent flow. Since the flow in the viscous sublayer, where bursting takes place, is mostly laminar, the modes of disturbance near the wall are likely to be similar to those for the laminar flow at a Reynolds number corresponding to the shear rate at the wall in the turbulent flow. A wall mode instability due to a compliant surface could alter the velocity profile in the wall region to a new nonparallel base state and affect the bursting phenomenon. In order to examine how the wall mode instability could affect the bursting phenomenon, it is first necessary to analyze the nature of finite amplitude bifurcating states near the point of transition, which is examined in the present study.

The wall elasticity renders the dynamics of flow past a compliant surface qualitatively different from that past a rigid surface at high Reynolds numbers. It is known that the compliant walls are useful in delaying the Tollmein–Schlichting instability in boundary-layer flow encountered in marine and aerospace applications.[8–11] For a flow through a gel-walled tube, the experimental evidence from Krindel and Silberberg[12] indicated that the drag force in a flexible tube is much larger than that in a rigid tube with the same radius at a Reynolds number where the flow in a rigid tube is laminar.

This anomalous drag force along with the visual observations led them to conclude that the onset of laminar to turbulence transition in a flow through a gel-walled tube can occur at a Reynolds number much smaller than 2100, the transition Reynolds number for flow through a rigid tube. Motivated by this observation, extensive studies centered around the linear stability analysis of fluid flow through tubes and channels bounded by compliant walls have been carried out. However, most of these studies are on the zero Reynolds number stability in the absence of inertia and the numerical extension of the results to finite Reynolds numbers.[13–16] An experimental confirmation of viscous instability can be found in Refs. 17–19. Even though the wall mode instability is likely to be very relevant in practical applications, very few studies have been carried out on the wall mode instability,[20–23] and all of these studies have been linear stability calculations. A linear stability analysis is inadequate because it only provides the transition Reynolds number but provides no information about the nature of the bifurcation after transition. In the present analysis, we present the first finite amplitude stability calculation of the wall mode instability in the flow past flexible surfaces. This is a first step toward the full nonlinear analysis of the wall modes in flow past compliant surfaces. The results of the present analysis provide the nature of the initial bifurcation and have the potential to provide further insights into the high Reynolds number transition and drag reduction process in the flow past soft materials.

Previous studies on wall mode instability have been restricted to the linear stability analysis of a flow past a solid surface which has been modeled as a linear elastic medium. The generalization of the classical linear elastic constitutive equation is the neo-Hookean rheological model valid for finite displacement gradients, featuring additional stresses nonlinear in solid strain.[24] Recently, many linear stability analyses have been revisited for the neo-Hookean description of the deformable medium, motivated by the finding of qualitatively different modes excited by the nonzero normal-stress difference present in the constitutive model.[25–29] There are two principal objectives of the present analysis: the use of the neo-Hookean constitutive relation for the solid and the weakly nonlinear analysis to determine whether the instability is of a super- or subcritical nature by calculating the finite amplitude correction to the linear growth rate in the Landau equation. The nonlinear contribution to the growth rate, the first Landau constant, is calculated numerically for a wide range of Reynolds numbers covering the regimes $\mathrm{Re} \ll 1$, the intermediate Reynolds number, and $\mathrm{Re} \gg 1$. The behavior in the regime $\mathrm{Re} \gg 1$ is also analyzed using the asymptotic analysis to verify the numerical results and also to provide the scalings of various quantities with respect to the Reynolds number.

II. PROBLEM FORMULATION

The system consists of an incompressible Newtonian fluid with density ρ and viscosity η occupying the domain $0 < y^* < R$. An incompressible deformable solid medium with thickness HR, shear modulus G, and density ρ is placed beneath the fluid. For simplicity the density of solid is assumed to be the same as that of the flowing fluid. This is a reasonable assumption for deformable walls made up of aqueous polymeric gels, like the ones used in the experiments,[17–19] where the densities of the fluid and the gel are comparable. In the experiments by Muralikrishnan and Kumaran,[18] the solid-to-fluid density ratio was 1.02. The rigid wall at $y^* = R$ is set moving in the x direction with velocity V and the elastic solid medium is anchored at the bottom plate at $y^* = -HR$ which is held stationary. The base flow configuration and the coordinate system are shown in Fig. 1. Here and in what follows, the quantities with a superscript $*$ are dimensional and the ones without the superscript are dimensionless unless stated otherwise. For a high Reynolds number flow, we adopt the inviscid scalings where the velocity is scaled with $\sqrt{G/\rho}$, distance with R, and time with $R\sqrt{\rho/G}$, and pressure and stresses in fluid as well as in solid wall are scaled with G. The dimensionless fluid continuity and momentum balance equations are

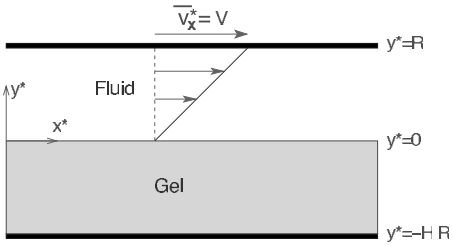

FIG. 1. Schematic diagram of plane Couette flow over a flexible surface showing the dimensional coordinate system.

$$\nabla \cdot \mathbf{v} = 0, \tag{1}$$

$$\partial_t \mathbf{v} + \mathbf{v} \cdot \nabla \mathbf{v} = \nabla \cdot \boldsymbol{\tau}, \tag{2}$$

where $\mathbf{v}$ denotes the fluid velocity field and the fluid stress tensor is of the form

$$\boldsymbol{\tau} = -p_f \mathbf{I} + \frac{\Gamma}{\mathrm{Re}}[\nabla \mathbf{v} + (\nabla \mathbf{v})^T], \tag{3}$$

where p_f is the fluid pressure, $\mathbf{I}$ is the identity tensor, and superscript T indicates the transpose. The Reynolds number is defined as $\mathrm{Re} = \rho V R/\eta$ and $\Gamma = \sqrt{\rho V^2/G}$ is the dimensionless top plate velocity.

The flexible medium is modeled as an incompressible neo-Hookean elastic solid continuum. The neo-Hookean model is a generalization of the linear elastic model used by Shankar and Kumaran[22,23] and incorporates the finite displacement gradient in the solid. This model has been used in the previous studies of linear stability analysis by Gkanis and Kumar,[25,26] although they preferred to use the Lagrangian description to model the solid dynamics against the Eulerian framework considered in the present analysis. In the Eulerian description, the dynamics of the solid wall is described by a displacement field $\mathbf{u}$, given by the displacement of a particle from an initial reference configuration $\mathbf{X}$ to a configuration $\mathbf{x}$ at any time t:

$$\mathbf{x} = \mathbf{X} + \mathbf{u}(\mathbf{x},t). \tag{4}$$

The deformation tensor in spatial configuration is given by

$$\mathbf{f} = \frac{\partial \mathbf{X}}{\partial \mathbf{x}} = (\mathbf{I} - \nabla \mathbf{u}). \tag{5}$$

The mass conservation condition for an incompressible solid is given by either

$$\text{Det } \mathbf{f} = 1 \tag{6}$$

or

$$\nabla \cdot \mathbf{v}^g = 0, \tag{7}$$

where Det indicates the determinant and $\mathbf{v}^g$ is the dimensionless Eulerian velocity field in the solid medium given by

$$\mathbf{v}^g = \partial_t \mathbf{u} + \mathbf{v}^g \cdot \nabla \mathbf{u}. \tag{8}$$

Both the above mass balance equations result in the following continuity condition:

$$\partial_x u_x + \partial_y u_y - \partial_x u_x \partial_y u_y + \partial_x u_y \partial_y u_x = 0. \tag{9}$$

The dimensionless momentum balance equation for the solid medium is

$$\partial_t \mathbf{v}^g + \mathbf{v}^g \cdot \nabla \mathbf{v}^g = \nabla \cdot \boldsymbol{\sigma}. \tag{10}$$

The total stress tensor in the gel comprises an isotropic gel pressure and an elastic contribution proportional to the strain ($\mathbf{e}$). As the gel is considered to be a neo-Hookean elastic solid, the viscous dissipation proportional to the strain rate ($\dot{\mathbf{e}}$) is ignored in the present analysis. The constitutive relation for the dimensionless stress, scaled with the shear modulus G, is

$$\boldsymbol{\sigma} = -p_g \mathbf{I} + 2\mathbf{e}. \tag{11}$$

The dissipative contribution to the total stress tensor, which is given in the dimensionless form as $(\eta_g/\eta)(\Gamma/\mathrm{Re})\dot{\mathbf{e}}$, is proportional to $\mathrm{Re}^{-2/3}$, as Γ for the wall modes scales as $\mathrm{Re}^{1/3}$ in the limit $\mathrm{Re} \gg 1$. Therefore, the viscous stresses due to the gel viscosity η_g are small and hence not accounted in the present analysis of wall mode instability. The strain tensor in the neo-Hookean elastic solid is given by[24]

$$\mathbf{e} = \tfrac{1}{2}(\mathbf{I} - \mathbf{f}^T \cdot \mathbf{f}) \tag{12}$$

or

$$e_{ij} = \frac{1}{2}\left(\frac{\partial u_i}{\partial x_j} + \frac{\partial u_j}{\partial x_i} - \frac{\partial u_k}{\partial x_i}\frac{\partial u_k}{\partial x_j}\right). \tag{13}$$

Here the terms quadratic in displacement gradient are the finite deformation stresses specific to the neo-Hookean model.

For the steady-state base flow shown in Fig. 1, the fluid velocity and the gel displacement field are

$$\bar{\mathbf{v}} = [\Gamma y, 0, 0],$$

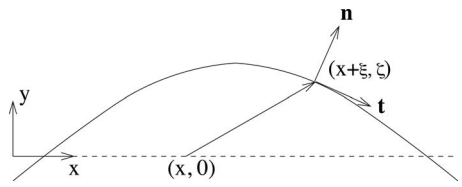

FIG. 2. Schematic illustrating the perturbed fluid-solid interface.

$$\bar{\mathbf{u}} = \left[\frac{\Gamma^2}{\mathrm{Re}}(y+H), 0, 0\right],$$

where Γ, the dimensionless velocity of the top plate, is the fluid shear rate. The stresses in the fluid and the gel medium are

$$\bar{\tau}_{xy} = \frac{\Gamma^2}{\mathrm{Re}}, \quad \bar{\tau}_{xx} = -\bar{p}_f, \quad \bar{\tau}_{yy} = -\bar{p}_f, \tag{14}$$

$$\bar{\sigma}_{xy} = \frac{\Gamma^2}{\mathrm{Re}}, \quad \bar{\sigma}_{xx} = -\bar{p}_g, \quad \bar{\sigma}_{yy} = -\bar{p}_g - \frac{\Gamma^4}{\mathrm{Re}^2}. \tag{15}$$

In addition to $\bar{v}_x = \Gamma$ at $y=1$ and zero displacement for the grafted gel at $y=-H$, the base flow solution also satisfies the normal and tangential velocity and stress continuity conditions at the fluid-gel interface, which, for the undisturbed flow, is flat at $y=0$. The nonzero value of the first normal-stress difference $\bar{\sigma}_{xx} - \bar{\sigma}_{yy} = \Gamma^4/\mathrm{Re}^2$ for the elastic solid is a consequence of the neo-Hookean constitutive model which retains the terms quadratic in displacement gradient Γ^2/Re. This additional stress, which was absent in the previous analyses of linear viscoelastic solid,[13,22,23] is known to influence the linear stability of the base state in the limit $\mathrm{Re} \ll 1$, as found by Gkanis and Kumar.[25]

III. WEAKLY NONLINEAR ANALYSIS

In the temporal stability analysis, a normal mode perturbation is superimposed on the steady base flow, and the temporal rate of change in amplitude is calculated using the perturbative expansion of nonlinearities with disturbance amplitude as a small parameter. Apart from the convective nonlinearities in the fluid governing equation, the mass and momentum balance equations for the neo-Hookean solid also admit terms nonlinear in displacement gradients. Moreover, the nonlinearities also arise from the fluid-solid interface boundary conditions.[30] The occurrence of nonlinear terms in the boundary conditions is elucidated first. While the interface in the undisturbed flow is flat at $y=0$, its position in the perturbed flow is different and it has to be obtained as a part of solution. As illustrated schematically in Fig. 2, a material point $(x,0)$ on the undisturbed interface moves to a position $(x+\xi,\zeta)$ due to the perturbations, where ξ and ζ are Lagrangian displacements of the material point at the interface. The matching conditions at the perturbed interface are

$$(\mathbf{t} \cdot \mathbf{v})|_{x+\xi,\zeta} = (\mathbf{t} \cdot \mathbf{v}^g)|_{x+\xi,\zeta}, \tag{16}$$

$$(\mathbf{n} \cdot \mathbf{v})|_{x+\xi,\zeta} = (\mathbf{n} \cdot \mathbf{v}^g)|_{x+\xi,\zeta}, \tag{17}$$

$$(\mathbf{t} \cdot \boldsymbol{\tau} \cdot \mathbf{n})|_{x+\xi,\zeta} = (\mathbf{t} \cdot \boldsymbol{\sigma} \cdot \mathbf{n})|_{x+\xi,\zeta}, \tag{18}$$

$$(\mathbf{n}\cdot\boldsymbol{\tau}\cdot\mathbf{n})|_{x+\xi,\zeta} = (\mathbf{n}\cdot\boldsymbol{\sigma}\cdot\mathbf{n})|_{x+\xi,\zeta}, \tag{19}$$

where $\mathbf{n}$ and $\mathbf{t}$ are the unit vectors normal and tangent to the perturbed interface (see Fig. 2) defined as

$$\mathbf{n} = \frac{-(\partial\zeta/\partial x)\mathbf{e}_x + \mathbf{e}_y}{\sqrt{1+(\partial\zeta/\partial x)^2}}, \quad \mathbf{t} = \frac{\mathbf{e}_x + (\partial\zeta/\partial x)\mathbf{e}_y}{\sqrt{1+(\partial\zeta/\partial x)^2}}. \tag{20}$$

The surface force due to interfacial tension is ignored in the present study. Denoting by F and G the fluid and gel quantities respectively, the interface conditions have the following generic form:

$$F|_{x+\xi,\zeta} = G|_{x+\xi,\zeta}, \tag{21}$$

where ξ and ζ are obtained as a part of the solution. In a weakly nonlinear analysis, the amplitude of all the perturbation quantities is assumed to be small but finite. Consequently, the quantities at the perturbed interface $(x+\xi,\zeta)$ can be approximated by the Taylor expansion about their values at the unperturbed interface $(x,0)$. The generic expression of interface conditions (21) can be written as

$$\begin{aligned}&[F]_0 + [\partial_x F]_0\xi + [\partial_y F]_0\zeta + \tfrac{1}{2}[\partial_x^2 F]_0\xi^2 + \tfrac{1}{2}[\partial_y^2 F]_0\zeta^2 \\ &\quad + [\partial_x\partial_y F]_0\xi\zeta + \cdots \\ &= [G]_0 + [\partial_x G]_0\xi + [\partial_y G]_0\zeta + \tfrac{1}{2}[\partial_x^2 G]_0\xi^2 + \tfrac{1}{2}[\partial_y^2 G]_0\zeta^2 \\ &\quad + [\partial_x\partial_y G]_0\xi\zeta + \cdots,\end{aligned} \tag{22}$$

where $[\cdots]_0$ denote quantities evaluated at the unperturbed interface $(y=0)$. Here ξ and ζ are obtained using the following Taylor expansions:

$$\begin{aligned}\xi &\equiv u_x(x+\xi,\zeta,t) \\ &= [u_x]_0 + [\partial_x u_x]_0\xi + [\partial_y u_x]_0\zeta + \tfrac{1}{2}[\partial_x^2 u_x]_0\xi^2 + \tfrac{1}{2}[\partial_y^2 u_x]_0\zeta^2 \\ &\quad + [\partial_x\partial_y u_x]_0\xi\zeta + \cdots,\end{aligned} \tag{23}$$

$$\begin{aligned}\zeta &\equiv u_y(x+\xi,\zeta,t) \\ &= [u_y]_0 + [\partial_x u_y]_0\xi + [\partial_y u_y]_0\zeta + \tfrac{1}{2}[\partial_x^2 u_y]_0\xi^2 + \tfrac{1}{2}[\partial_y^2 u_y]_0\zeta^2 \\ &\quad + [\partial_x\partial_y u_y]_0\xi\zeta + \cdots.\end{aligned} \tag{24}$$

The expressions for ξ and ζ in terms of displacement components u_x and u_y and their derivatives evaluated at $y=0$ can be obtained from the above expansions up to a desired order of perturbation amplitude.

The Eulerian velocity field in the gel $(\mathbf{v}^g)$ is obtained to a desired order from the following expressions:

$$v_x^g = \partial_t u_x + v_x^g\partial_x u_x + v_y^g\partial_y u_x, \tag{25}$$

$$v_y^g = \partial_t u_y + v_x^g\partial_x u_y + v_y^g\partial_y u_y. \tag{26}$$

The theory of weakly nonlinear stability analysis is briefly discussed next. A two-dimensional perturbation with small but finite amplitude $A_1(\tau)$ with axial wavenumber α and wavespeed c (frequency $\omega=-\alpha c$) is superimposed on the base state at the critical condition. Here, τ is the slow time scale, which will be defined later. The dimensionless shear rate for critical stability is Γ_c such that for $\Gamma<\Gamma_c$ the flow is stable to perturbations with any wavelength. The critical point (α_c,Γ_c) and the frequency of this mode are obtained from the linear stability analysis. In the neighborhood of $\Gamma=\Gamma_c$, the dynamics are assumed to be dominated by the fundamental disturbance with wavenumber $\alpha=\alpha_c$ and its higher harmonics generated by the nonlinear self-interactions of the fundamental mode. In weakly nonlinear theory, the disturbance is expanded in a harmonic series and the quantity at each harmonic is further expanded in an asymptotic series with disturbance amplitude as a small parameter.[31,32] Using the definition $E(x,t)=\exp[i\alpha(x-ct)]$ for convenience, a general field ϕ is expanded as follows:

$$\begin{aligned}\phi(x,y,t) = \bar{\phi}(y) + \sum_{k=0}^{\infty}\sum_{n=k,n\neq 0}^{\infty}[A_1(\tau)]^n \\ \times[E^k\tilde{\phi}^{(k,n)}(y) + E^{-k}\tilde{\phi}^{(k,n)^\dagger}(y)],\end{aligned} \tag{27}$$

where the overbar represents the base flow quantity and the superscript † denotes the complex conjugate, and $\phi=[\mathbf{v},p_f,\mathbf{u},p_g]$. Here and in what follows, k denotes the harmonic index and n denotes the asymptotic order. The perturbation amplitude $A_1(\tau)$, which varies on the slow time scale τ, is a small parameter and is written as $A_1(\tau)=\epsilon A(\tau)$, where ϵ is the small parameter in the expansion and $A(\tau)\sim O(1)$. It should be noted that $A_1(\tau)$ is a real quantity since the temporal oscillations are included in $E(x,t)$.

In the vicinity of the point with critical stability, the disturbance amplitude is assumed to satisfy the following evolution equation known as the Landau equation:

$$A_1(\tau)^{-1}d_tA_1(\tau) = s_r^{(0)} + A_1(\tau)^2 s_r^{(1)} + \cdots, \tag{28}$$

where the constant $s_r^{(0)}$ is the real part of the linear growth rate $s^{(0)}$ which emerges as an eigenvalue from the classical linearized stability analysis. The linear growth rate is related to the wavespeed as $s^{(0)}=-i\alpha c$. The constant $s_r^{(1)}$ is the real part of the first Landau constant $s^{(1)}$. In the neighborhood of neutral stability, such that $\Gamma-\Gamma_c=\Gamma_2\epsilon^2\ll 1$, where ϵ is the order of magnitude of disturbance amplitude such that $A_1(\tau)=\epsilon A(\tau)$, we write $s_r^{(0)}=(\Gamma-\Gamma_c)(ds_r^{(0)}/d\Gamma)$. The slow time scale τ modifies the time derivative as $d_t\to d_t+\epsilon^2 d_\tau$. Hence, there exist multiple time scales in the system: a fast time scale (t) corresponding to the inverse of the frequency of oscillations and a slow time scale (τ) corresponding to the rate of growth or decay of the disturbance amplitude. Since the $A_1(\tau)$ is independent of the fast time scale t, the scaled dynamical equation for the amplitude becomes

$$A(\tau)^{-1}d_\tau A(\tau) = \Gamma_2\frac{ds_r^{(0)}}{d\Gamma} + A(\tau)^2 s_r^{(1)} + \cdots. \tag{29}$$

The imaginary part of the first Landau constant provides the correction of the perturbation frequency due to the nonlinear interactions:

$$\omega = s_i^{(0)} + \Gamma_2\frac{ds_i^{(0)}}{d\Gamma} + A(\tau)^2 s_i^{(1)} + \cdots, \tag{30}$$

where $s_i^{(0)}$ is the frequency of perturbations calculated from the linear stability analysis $(s_i^{(0)}=-\alpha c_r)$ and $s_i^{(1)}$ is the correction to the frequency of the perturbations due to self-interactions generated by the nonlinearities.

IV. CALCULATION OF THE LANDAU CONSTANT $s^{(1)}$

The objective of the rest of the analysis is to determine the first Landau constant $s^{(1)}$ which in turn reveals whether the nature of wall mode instability is supercritical ($s_r^{(1)}<0$) or subcritical ($s_r^{(1)}>0$). Upon expanding all the dynamical quantities in harmonic-amplitude series, as shown in Eq. (27), and extracting the governing equations at various orders, inhomogeneous terms appear in the fluid and the solid governing equations due to the nonlinearities. Moreover, the interfacial conditions at the perturbed interface, which are written in Taylor series expansion about the flat interface as in Eq. (22), introduce nonlinearities. In general, the governing equations and the boundary conditions for the problem at order (k,n) contain inhomogeneous terms of order (j,m), where $m<n$ and $j+m\leq k+n$. Thus, the harmonic-amplitude series expansion converts the original nonlinear fluid-gel problem with unknown interface into a hierarchy of linear but inhomogeneous problems each to be solved sequentially beginning with the $k=1$ and $n=1$ problem. An observation of governing equations at different orders shows that the eigenfunctions $\tilde{\phi}^{(k,n)}$ vanish if $k+n$ is odd. Thus, only a few remaining nonzero eigenfunctions need to be calculated. The first Landau constant, which is the first correction to linear growth rate, appears in the time derivative with fluid velocity $\mathbf{v}$ and gel velocity $\mathbf{v}^g$. In the hierarchy of problems at various orders, $s^{(1)}$ first appears in the problem with $k=1$ and $n=3$. Therefore, in the weakly nonlinear analysis, where the objective is to calculate only the first Landau constant $s^{(1)}$, only the equations for the (1,1), (0,2), (2,2), and (1,3) contributions need to be solved. The (1,1) problem is the linear stability problem which provides the critical point around which the harmonic-amplitude expansion is carried out, the (0,2) problem is $O(A_1^2)$ correction to the mean flow, often termed as the base flow distortion, the (2,2) problem is the first harmonic of the fundamental mode which manifests at order A_1^2, and the (1,3) problem is the nonlinear correction to the least stable fundamental mode, at which order the Landau equation (28) is recovered. The governing equations at various orders and the details of the solution procedure are provided in Appendix A.

V. RESULTS AND DISCUSSIONS

A. Linear stability analysis

Shankar and Kumaran[23] examined the stability of wall modes using the high Re asymptotics for a plane Couette flow past a deformable surface described as a linear elastic solid. In the present work, we extend the asymptotic analysis to a neo-Hookean elastic solid which accounts for finite strain deformations. The analysis balances the viscous and inertial forces in a thin layer adjacent to the fluid-solid interface with thickness $O(\mathrm{Re}^{-1/3})$ times the channel width in the limit $\mathrm{Re}\gg 1$. The outer fluid layer is considered to be inviscid and the disturbance vorticity is confined to the wall layer. The governing equations are expanded using the small parameter $\delta=\mathrm{Re}^{-1/3}$. The fluid shear rate is scaled as $\Gamma=\Gamma_0\mathrm{Re}^{1/3}$, and the wavespeed is written as $c=c_0+c_1\delta+\cdots$, where Γ_0 is of $O(1)$ quantity. The governing equations and the interface conditions at the leading order and their first correction are provided, along with the solution procedure, in Appendix B. The eigenvalue problem at the leading order provides the leading order wavespeed c_0 as the eigenvalue. There are multiple solutions for c_0, all of which have zero imaginary part. Thus, the leading order solutions do not exhibit an instability. At the next order we get the value of c_1, the first correction to the wavespeed. For all of the multiple values of c_0, the resultant c_1 is found to be a complex number for a given value of Γ_0. Thus, by setting the imaginary part c_{i1} to zero, the value of scaled transitional shear rate Γ_0 can be obtained. Transitional Γ_0 for the multiple values of c_0 are characterized as different modes belonging to the class of wall modes. Table I shows the results of the asymptotic analysis and compares with the solutions obtained by Shankar and Kumaran[23] for the Hookean solid for $H=5$ and $\alpha=1$. Since the finite strain terms specific to the neo-Hookean model are proportional to the base-state strain in the solid (Γ^2/Re), which is of magnitude $O(\delta)$, the leading order eigenvalue c_0 is identical with that for the linearly elastic solid. However, the finite strain deformations alter the value of c_1, and, hence, the transition parameter Γ_0 is different for the linear and neo-Hookean models. Unlike for the linear elastic solid, the upstream traveling disturbances for the neo-Hookean solid do become unstable, as previously observed by Gkanis and Kumar[25,26] for the creeping flow. Of all the modes, the most unstable mode, however, is the downstream traveling mode 1-d and for this mode the value of transition parameter Γ_0 is found to be only marginally larger than that for the linear elastic solid.

TABLE I. The asymptotic solutions, leading order wavespeed c_0, and transition parameter Γ_0 for the first four wall modes in the limit $\mathrm{Re}\gg 1$ keeping $H=5$ and $\alpha=1$. The table compares the results for the Hookean solid analyzed in Ref. 23 with that for the neo-Hookean solid analyzed in the present study. c_0 is the same for both the models. Here, d indicates the downstream traveling mode and u the upstream traveling mode (which means negative wavespeed).

		Γ_0	
	Leading order wavespeed c_0	Hookean solid	Neo-Hookean solid
Mode 1-d	1.254 84	0.590 49	0.599 80
Mode 1-u	−1.254 84	Stable	1.617 73
Mode 2-d	1.761 42	0.928 11	1.038 49
Mode 2-u	−1.761 42	Stable	1.831 98
Mode 3-d	2.335 53	2.628 20	Stable
Mode 3-u	−2.335 53	Stable	2.109 86
Mode 4-d	2.933 56	3.806 13	Stable
Mode 4-u	−2.933 56	Stable	2.466 18

The asymptotic solutions valid for $\mathrm{Re}\gg 1$ can be continued to small Reynolds number using the numerical continuation. The governing equations for the numerical solution are provided in Appendix A 1 and the numerical scheme is explained in detail in Ref. 15. Using the transitional shear rate Γ, the stability diagram is constructed in terms of a flow independent parameter, $\Sigma=\rho GR^2/\eta^2$, which is calculated following the definition $\Sigma=\mathrm{Re}^2/\Gamma^2$. Figure 3 shows the typi-

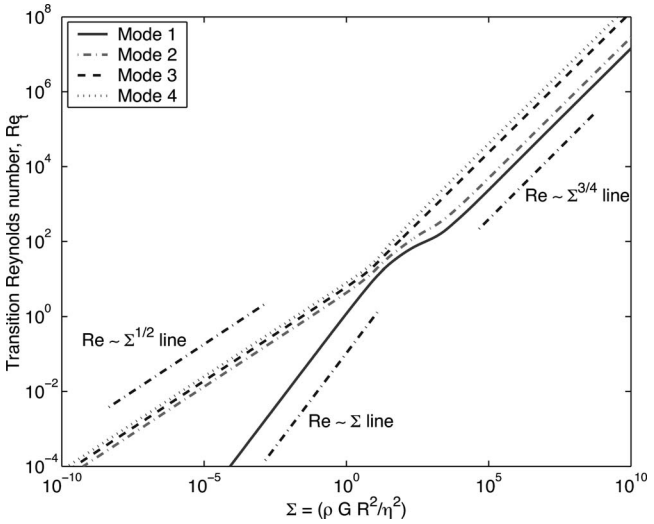

FIG. 3. The neutral stability curves for different wall modes obtained from the numerical continuation of the asymptotic results for the linearly elastic solid for $H=5$ and $\alpha=1$.

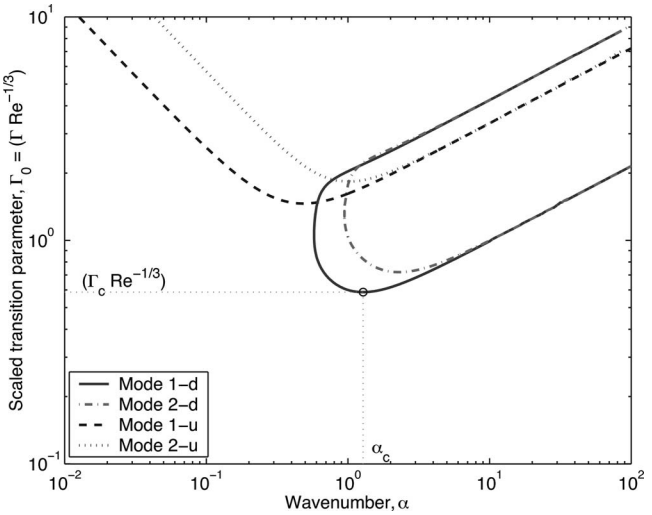

FIG. 5. Variation in the scaled transition parameter Γ_0, obtained from the asymptotic analysis, with the axial wavenumber for the first two modes for $\mathrm{Re}\gg 1$ and $H=5$. The point of minimum Γ_0 provides the critical parameters $(\Gamma_c\,\mathrm{Re}^{-1/3})$ and α_c.

cal neutral stability diagram in the Re-Σ plane for $H=5$ and $\alpha=1$ for the linear elastic solid. This figure, which is reproduced from the earlier studies,[23] shows the behavior of the first four wall modes with Reynolds number for the linear elastic solid. The wall modes are characterized by the scaling $\mathrm{Re}\sim\Sigma^{3/4}$ for $\Sigma\gg 1$, which follows from the definition $\Sigma=\mathrm{Re}^2/\Gamma^2$ and the scaling $\Gamma\sim\mathrm{Re}^{1/3}$. The most unstable mode 1 continues to small Reynolds numbers and agrees with the unstable viscous mode studied by Kumaran *et al.*[13] The corresponding diagram for the neo-Hookean solid is illustrated in Fig. 4 which shows the numerical continuations of the first two wall modes to small Reynolds numbers in the Re-Σ plane for $H=5$ and $\alpha=1$. As the two branches of the downstream traveling modes merge with each other and both the upstream traveling modes stabilize as the Reynolds number approaches zero (indicated by the scaling law $\mathrm{Re}\sim\Sigma^{1/2}$) for this case, the stability curve is also shown for a different wavenumber $\alpha=2$. Here, the continuation of the most unstable wall mode to small Reynolds number is demonstrated by the gray shaded line and the scaling behavior $\mathrm{Re}\sim\Sigma$ in the limit $\Sigma\ll 1$ is shown.

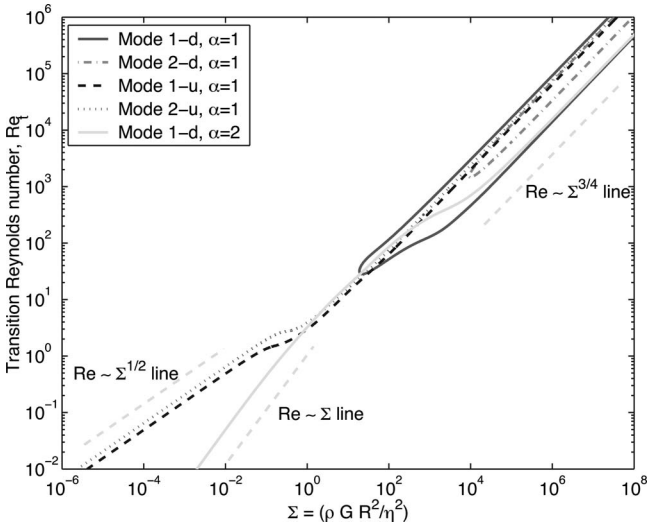

FIG. 4. The neutral stability curves in the Re-Σ plane for the first two wall modes obtained from the numerical continuation of the asymptotic results for the neo-Hookean elastic solid for $H=5$ and $\alpha=1$. The gray shaded line shows the behavior of mode 1-d for wavenumber $\alpha=2$. Here, d indicates the downstream traveling mode and u represents the upstream traveling mode (which means negative wavespeed).

The variation in $\Gamma_0=\Gamma\,\mathrm{Re}^{-1/3}$ with wavenumber α from the asymptotic analysis for the first two downstream and upstream modes is shown in Fig. 5 for $H=5$. The point of minimum Γ_0 on this diagram provides the critical parameter $(\Gamma_c\,\mathrm{Re}^{-1/3})$ and the critical wavenumber α_c. Figure 6 plots the critical parameter $\Gamma_c\,\mathrm{Re}^{-1/3}$ and the critical wavenumber α_c as a function of dimensionless solid thickness H. The figure compares the asymptotically obtained $\Gamma_c\,\mathrm{Re}^{-1/3}$ and α_c (indicated by solid line) with the same calculated numerically for a finite Reynolds number, $\mathrm{Re}=10^4$ ($\triangle$ symbols) and $\mathrm{Re}=10^6$ ($\bigcirc$ symbols). As shown, the asymptotic solution agrees well with the numerical solution for $\mathrm{Re}=10^6$, whereas for $\mathrm{Re}=10^4$, the asymptotic solution does not hold for $H<1$. The figure also compares the asymptotic solution for the neo-Hookean elastic solid with that for the linearly elastic solid medium (indicated by $\square$ symbols). Note that $\Gamma_c\,\mathrm{Re}^{-1/3}$ obtained for both the models in the limit $\mathrm{Re}\gg 1$ is in good agreement for all values of H considered in the analysis, which corroborates the fact that the finite strain deformations do not play a significant role in the wall mode instability for $\mathrm{Re}\gg 1$.

Figure 7 shows a numerically obtained stability diagram showing the critical Reynolds number as a function of the fluid-solid system parameter Σ for $H=1$. The disturbance wavenumber along the diagram is α_c, the critical wavenumber for a given Re. The asymptotically obtained diagram is shown to hold for Reynolds numbers as low as $\mathrm{Re}=10^4$. For comparison, the results obtained for the linearly elastic solid are also plotted. The wall mode scaling $\mathrm{Re}\sim\Sigma^{3/4}$ smoothly changes to $\mathrm{Re}\sim\Sigma$ for $\mathrm{Re}\ll 1$, in which regime we recover

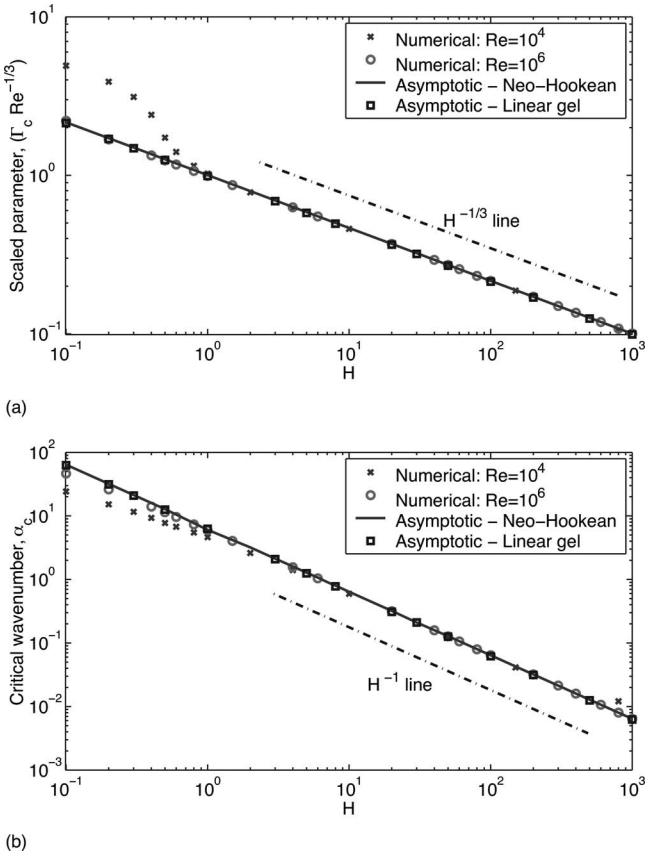

FIG. 6. Effect of solid thickness H on (a) the critical shear rate Γ_c scaled with Re; (b) the critical wavenumber α_c. The critical parameters obtained from the high Re asymptotics are compared with the numerical results for $\mathrm{Re}=10^4$ and 10^6 and also with the asymptotic solutions for the linear elastic solid.

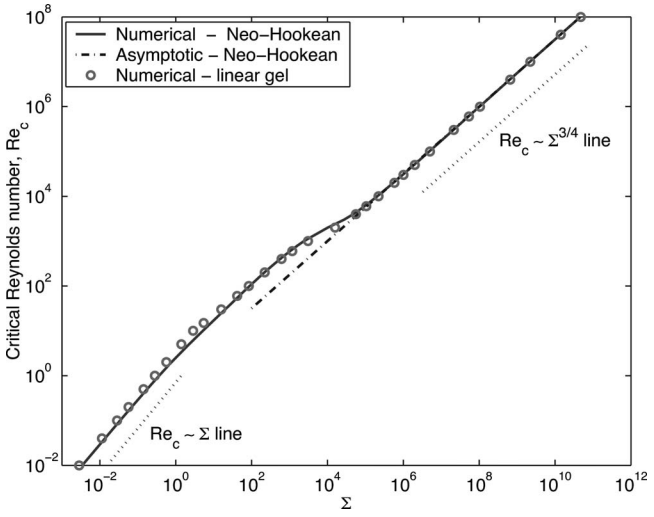

FIG. 7. Comparison of the numerical results, the critical Reynolds number as a function of Σ, obtained from the present analysis of the neo-Hookean solid (solid line) with the numerical results for the linear elastic solid analyzed in Ref. 15 (symbols) for $H=1$. The dot-dashed line shows the asymptotic results for the neo-Hookean solid which agrees with the numerical results for $\mathrm{Re}\geq 10^4$. The dotted lines are the reference lines showing different scaling behaviors.

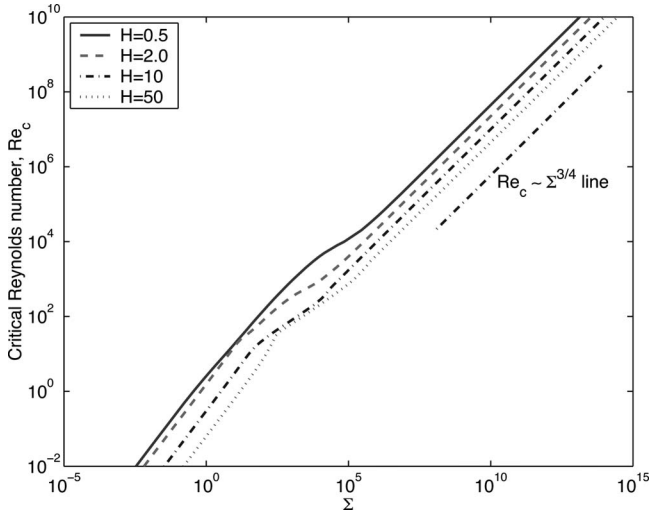

FIG. 8. The critical stability diagram for the neo-Hookean solid showing the critical Reynolds number as a function of Σ for different values of solid thickness H.

the unstable viscous instability analyzed by Gkanis and Kumar.[25] Figure 8 shows the similar diagrams for different values of solid thickness H. For a given fluid-solid system, characterized by Σ, the critical Reynolds number decreases as the thickness ratio H increases following the scaling $\mathrm{Re}_c \sim H^{-1/2}$ for $\mathrm{Re}\gg 1$. Thus, the thick solids are relatively easier to destabilize by the wall mode perturbations.

An important observation from the linear stability analysis is that for $\mathrm{Re}\gg 1$ the critical shear rate for the neo-Hookean elastic solid is very close to that for the linear elastic solid for the entire range of solid-to-fluid thickness ratios considered in the present study. The scalings used in the asymptotic analysis can provide further insights. The additional stresses generated by finite strain deformations are proportional to the base-state strain in solid which is Γ^2/Re. As $\Gamma \sim \mathrm{Re}^{1/3}$ in the limit $\mathrm{Re}\gg 1$, the additional neo-Hookean contribution is $O(\mathrm{Re}^{-1/3})$. However, since the transition shear rate is recovered at order $\mathrm{Re}^{-1/3}$, these additional stresses could influence the transition point. As suggested by the energy balance arguments of Kumaran,[20] the instability occurs when the transfer of energy from the mean flow to the fluctuations due to the shear work done by the fluid at the interface exceeds the rate of viscous dissipation of energy in the wall layer. The total energy of perturbations is given by

$$\frac{d\mathcal{E}}{dt} = \mathcal{C} + \mathcal{S} - \mathcal{D}, \tag{31}$$

where disturbance energy $\mathcal{E}$ is the sum of the kinetic energy of motion in fluid and solid and the elastic strain energy stored in the solid. $\mathcal{C}$ is the rate of transfer of energy from mean flow to fluctuations by convective terms in the momentum equations, $\mathcal{S}$ is the rate of transfer of energy due to the shear work done by mean flow at the interface, and $\mathcal{D}$ is the total rate of viscous dissipation of disturbance energy in fluid as well as solid. When the solid is treated purely as an elastic medium without taking into account the viscous dissipation, as in the present work (see Sec. II), the dissipation occurs

only in the fluid. The rate of shear work done at the interface is given by the expression

$$\mathcal{S} = \int \mathbf{n}\cdot\boldsymbol{\tau}\cdot\mathbf{v}|_{\text{fluid}}dx + \int \mathbf{n}\cdot\boldsymbol{\sigma}\cdot\mathbf{v}^{g}|_{\text{solid}}dx. \tag{32}$$

At the leading order, we have

$$\mathcal{S} = -\int (\tau'_{xy}v'_x + \tau'_{yy}v'_y)dx + \int (\sigma'_{xy}v_x^{g'} + \sigma'_{yy}v_y^{g'})dx. \tag{33}$$

The quantities with primes are the perturbation quantities. The integrals in the above expression are to be carried out at $y=0$ over one wavelength of disturbance along the x direction. The interface conditions as given in Eqs. (A6)–(A9) are

$$v'_y = v_y^{g'}, \quad v'_x + \bar{\dot{\gamma}}u'_y = v_x^{g'}, \tag{34}$$

$$\tau'_{yy} = \sigma'_{yy}, \quad \tau'_{xy} + \bar{N}_1(\partial u'_y/\partial x) = \sigma'_{xy}. \tag{35}$$

Here, the base-state shear rate $\bar{\dot{\gamma}}=\Gamma$ and the first normal-stress difference $\bar{N}_1=\Gamma^4/\mathrm{Re}^2$. Using the above equalities, the expression for the rate of work done at the interface becomes

$$\mathcal{S} = -\int_0^{2\pi/\alpha} \bar{\dot{\gamma}}u'_y\sigma'_{xy}dx + \int_0^{2\pi/\alpha} \bar{N}_1(\partial u'_y/\partial x)v'_x dx \tag{36}$$

$$= \frac{2\pi}{\alpha}\Gamma(\tilde{u}_y\tilde{\sigma}^{\dagger}_{xy} + \tilde{u}^{\dagger}_y\tilde{\sigma}_{xy}) + \frac{2\pi}{\alpha}\frac{\Gamma^4}{\mathrm{Re}^2}(i\alpha\tilde{u}_y\tilde{v}^{\dagger}_x - i\alpha\tilde{u}^{\dagger}_y\tilde{v}_x). \tag{37}$$

As there is no normal-stress difference, the second term is absent for the linear (Hookean) elastic solid. Additionally, the neo-Hookean expression for the shear stress, that is, $\tilde{\sigma}_{xy}=i\alpha\tilde{u}_y+d_y\tilde{u}_x-(\Gamma^2/\mathrm{Re})i\alpha\tilde{u}_x$, contains an additional term proportional to Γ^2/Re not present in the Hookean solid. Thus, we may split $\mathcal{S}$ into the Hookean and the non-Hookean contributions. The latter is made up of contributions due to the additional finite deformation stress and due to the jump in the first normal-stress difference across the interface:

$$\mathcal{S} = \mathcal{S}_H + \frac{2\pi}{\alpha}\frac{\Gamma^2}{\mathrm{Re}}\Gamma(i\alpha\tilde{u}_y\tilde{u}^{\dagger}_x - i\alpha\tilde{u}^{\dagger}_y\tilde{u}_x) + \frac{2\pi}{\alpha}\frac{\Gamma^4}{\mathrm{Re}^2}(i\alpha\tilde{u}_y\tilde{v}^{\dagger}_x - i\alpha\tilde{u}^{\dagger}_y\tilde{v}_x) \tag{38}$$

$$= \mathcal{S}_H + \mathcal{S}_1 + \mathcal{S}_2. \tag{39}$$

In the perturbation energy balance Eq. (31), the contribution due to convection turns out to be subdominant.[20] The instability occurs when the rate of shear work done at the interface, $\mathcal{S}$, exceeds the rate of dissipation, $\mathcal{D}$. For nondissipating solids, the dissipation occurs only in the fluid and its expression remains the same irrespective of the type of constitutive model used to describe the solid. We are interested only in the role of neo-Hookean terms additional to the Hookean solid, and hence we do not evaluate the dissipation term $\mathcal{D}$. Since the neo-Hookean contributions influence only the destabilizing term $\mathcal{S}$, we examine the relative contribution $\mathcal{S}/\mathcal{S}_H=1+\mathcal{S}_1/\mathcal{S}_H+\mathcal{S}_2/\mathcal{S}_H$ as a function of the Reynolds number for a neutrally stable wall mode. Figure 9 plots the ratio of the transition shear rate for the neo-Hookean solid to that for the Hookean solid, Γ/Γ_H, and also the relative contribution of the shear work done at the interface, $\mathcal{S}/\mathcal{S}_H$. For viscous instability in the limit $\mathrm{Re}\ll 1$, the ratio $\Gamma/\Gamma_H<1$. This can be attributed to the higher extent of shear deformation work at the interface for the neo-Hookean solid. For $\mathrm{Re}\gg 1$, the ratio Γ/Γ_H becomes greater than unity because the surface work contribution to the energy balance becomes smaller than that for the Hookean solid ($\mathcal{S}/\mathcal{S}_H<1$). Since $\mathcal{S}/\mathcal{S}_H=1+\mathcal{S}_1/\mathcal{S}_H+\mathcal{S}_2/\mathcal{S}_H$, Fig. 9 shows that this crossover is largely due to the change in sign of the term $\mathcal{S}_1/\mathcal{S}_H$, which is the contribution of the additional finite deformation stresses in the neo-Hookean solid. Importantly, the contribution of the normal-stress difference $\mathcal{S}_2/\mathcal{S}_H$ is insignificant at high Reynolds numbers. It should be noted that this contribution plays an important role in shortwave instability at $\mathrm{Re}\ll 1$,[25] for which case the ratio $\mathcal{S}_2/\mathcal{S}_H$ is found to be positive and much greater than $\mathcal{S}_1/\mathcal{S}_H$.

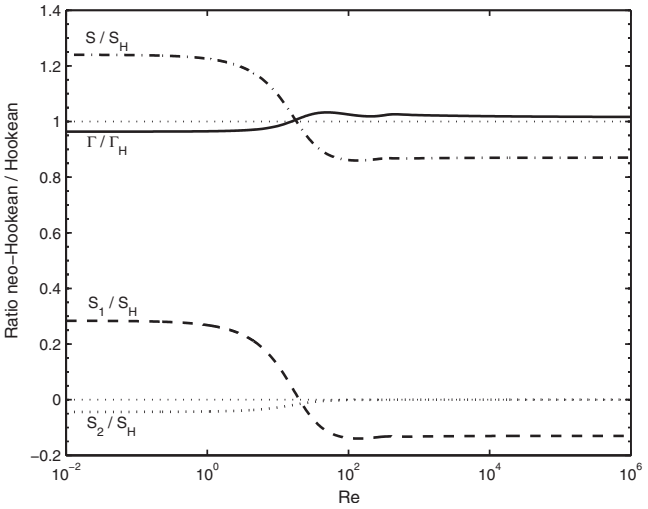

FIG. 9. The ratio of quantities for the neo-Hookean elastic solid to that for the Hookean elastic solid: transition shear rate Γ/Γ_H and rate of shear work done at the interface $\mathcal{S}/\mathcal{S}_H$ plotted as a function of Reynolds number for $H=10$ and $\alpha=0.5$. Two neo-Hookean contributions to $\mathcal{S}/\mathcal{S}_H$, $\mathcal{S}_1/\mathcal{S}_H$, and $\mathcal{S}_2/\mathcal{S}_H$ are also plotted. The change in sign of the first contribution leads to the crossover from destabilizing to stabilizing influence of the neo-Hookean terms on shear rate.

B. Nonlinear stability analysis

1. Numerical analysis

The shooting method used to solve the linear stability problem provides accurate eigenvalues for any arbitrary Reynolds number. This is possible due to the Gram–Schmidt orthogonalization of solutions carried out at all grid points.[15] However, the estimation of eigenfunctions becomes error prone for $\mathrm{Re}\gtrsim 1000$, especially for the inhomogeneous problem at order (2,2). Hence, we use the spectral method for the nonlinear stability analysis. The computational technique is validated by recovering the known results for the viscous mode instability.[33] The formulations and the solution procedure are described in Appendix A.

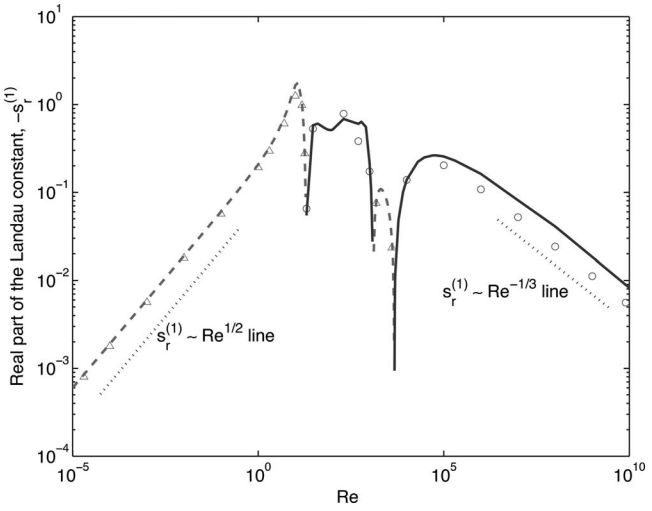

FIG. 10. Variation in the real part of the Landau constant $-s_r^{(1)}$ with Reynolds number for $H=10$. The transition parameters along the curve are Γ_c and α_c. The broken line is used when $s_r^{(1)}$ is positive and solid line is used to represent the case where $s_r^{(1)}$ is negative. The symbols indicate the Landau constant $-s_r^{(1)}$, for a linear elastic solid: △ for subcritical and ○ for supercritical bifurcation.

The Landau constant $s^{(1)}$, calculated in the vicinity of the critical point (Γ_c, α_c), is plotted in Fig. 10 for a wide range of Reynolds numbers starting from $\mathrm{Re} \ll 1$ to $\mathrm{Re}=10^{10}$ for $H=10$. Here, the broken line indicates that $s_r^{(1)}>0$ and the solid line is used to represent the case where $s_r^{(1)}<0$. For the viscous instability in the limit $\mathrm{Re} \ll 1$, the real part of the Landau constant $s_r^{(1)}$ is found to be positive, indicating the subcritical nature of the bifurcation, as mentioned by Shankar and Kumaran.[33] In this regime, the Landau constant $s_r^{(1)}$, scaled by $(G/\rho R^2)^{1/2}$, is proportional to $\mathrm{Re}^{1/2}$. For intermediate Reynolds numbers, $s_r^{(1)}$ changes its sign three times, and finally it remains negative for $\mathrm{Re} \gg 1$. Thus, the nature of bifurcation of the high Reynolds number wall mode instability is supercritical. In the regime $\mathrm{Re} \gg 1$, the Landau constant follows the scaling $s_r^{(1)} \sim \mathrm{Re}^{-1/3}$. Also shown in Fig. 10 is the Landau constant $s_r^{(1)}$ for a case when the flexible solid is modeled as a linear elastic solid (indicated by symbols △ for subcritical and ○ for supercritical bifurcation). While the quantitative value of the Landau constant is somewhat different, the range of Reynolds numbers for which the bifurcation is either subcritical or supercritical appears to be the same for both the solid models. Thus, the neo-Hookean nonlinearities in solid do not influence the changes in the sign of the Landau constant for varying Reynolds numbers. The balance between the nonlinearities arising due to the perturbed interface and the convective nonlinearities in the fluid momentum equation, therefore, determines the crossover from the subcritical transition for $\mathrm{Re} \ll 1$ to the supercritical stability for $\mathrm{Re} \gg 1$. This knowledge of the response of the nonlinearities for a wide range of Reynolds numbers can be useful in deciding the operating conditions of flow systems depending on the choice of the nature of bifurcation. For a subcritical transition, the destabilizing influence of nonlinearities renders the flow unstable at shear rates lower than Γ_c predicted by the linear stability. A supercritical bifurcation makes it possible to achieve the controlled transition through stable nonlaminar secondary motions.

An important quantity in finite amplitude stability analysis is the equilibrium amplitude for which the linear growth rate and its nonlinear correction balance each other in the neighborhood of the critical point. The expression of the equilibrium amplitude, obtained from the scaled Landau equation near $\Gamma=\Gamma_c$ [Eq. (29)] by setting $dA/d\tau=0$, is given as

$$A_e^2 = \frac{-(ds_r^{(0)}/d\Gamma)\Gamma_2}{s_r^{(1)}}. \tag{40}$$

Noting that the actual amplitude $A_1=\epsilon A$ and $\Gamma-\Gamma_c=\epsilon^2\Gamma_2$, the equilibrium amplitude is

$$A_{1e}^2 = \frac{-(ds_r^{(0)}/d\Gamma)(\Gamma-\Gamma_c)}{s_r^{(1)}}. \tag{41}$$

For $s_r^{(1)}>0$, A_{1e}^2 is positive for $\Gamma<\Gamma_c$, and for $s_r^{(1)}<0$, the positive amplitude exists for $\Gamma>\Gamma_c$. For a subcritical bifurcation, the equilibrium amplitude represents the threshold disturbance amplitude of the unstable branch for $\Gamma<\Gamma_c$, and for a supercritical bifurcation, the equilibrium amplitude represents the amplitude of the stable nonlaminar states superimposed on the laminar flow, thus indicating the extent of distortion of the mean flow that is realized for $\Gamma>\Gamma_c$. It is important to note here that the numerical values of the Landau constant, and hence the values of A_{1e}^2, depend on the normalization condition used to obtain the eigenfunctions for the problem at order (1,1). In the present study, the normalization condition $\tilde{u}_x^{(1,1)}=1+i$ at $y=0$ has been used. However, any perturbation quantity of the form $A_{1e}\tilde{\phi}(y)e^{(i\alpha x+s^{(0)}t)}$ will be independent of the normalization condition employed. One such quantity of interest is the normal displacement of the fluid-solid interface given by the following expression, correct to $O(\epsilon)$:

$$|u_y'|_{y=0} = A_{1e}|\tilde{u}_y^{(1,1)}|_{y=0}. \tag{42}$$

Figure 11 shows the equilibrium amplitude in the form $A_{1e}/\sqrt{\Gamma-\Gamma_c}$ and the amplitude of the normal displacement of interface in the form $|u_y'|_{y=0}/\sqrt{\Gamma-\Gamma_c}$ as a function of the flow Reynolds numbers for $H=10$. Here, the solid lines with symbols represent the case $s_r^{(1)}<0$ and the broken lines with symbols indicate the regime with subcritical instability. The equilibrium amplitude diverges when $s_r^{(1)}$ passes through zero during the three sign changes. The equilibrium amplitude $A_{1e}/\sqrt{\Gamma-\Gamma_c}$ scales as $\mathrm{Re}^{-1/6}$ for $\mathrm{Re} \gg 1$; thus $A_{1e}^2/(\Gamma-\Gamma_c) \sim \delta$ in the same limit. Here, $\delta=\mathrm{Re}^{-1/3}$ is the thickness of the wall layer confining the disturbance vorticity. The normal displacement of an interfacial point is found to decrease proportionally to $\mathrm{Re}^{-1/2}$ in the limit $\mathrm{Re} \gg 1$. Thus, the unstable flow for $\Gamma>\Gamma_c$ reaches the supercritically bifurcated stationary state, which resembles more and more the laminar base state as the flow Reynolds number increases. Figure 12 plots the real part of the Landau constant against the flow Reynolds number for different values of solid thickness H. For

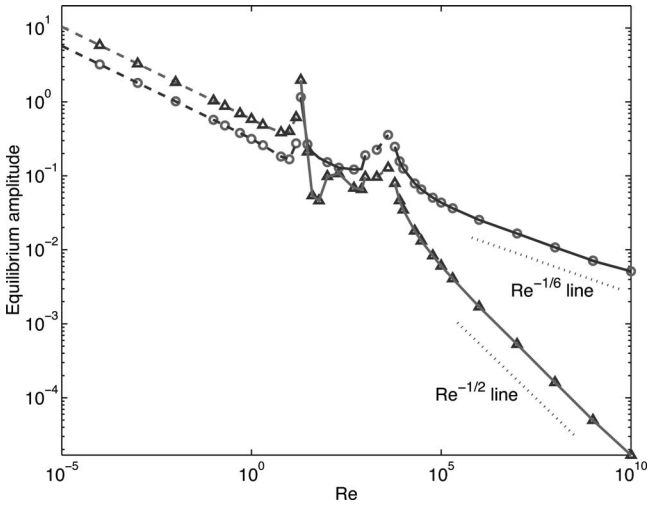

FIG. 11. Variation in the equilibrium amplitude $A_{1e}/\sqrt{\Gamma-\Gamma_c}$ (○) and the amplitude of the normal displacement of the fluid-solid interface $|u_y'|_{y=0}/\sqrt{\Gamma-\Gamma_c}$ (△) with the Reynolds number for $H=10$. The amplitudes diverge when $s_r^{(1)}$ passes through zero. The broken line is used when $s_r^{(1)}$ is positive and the solid line when $s_r^{(1)}$ is negative.

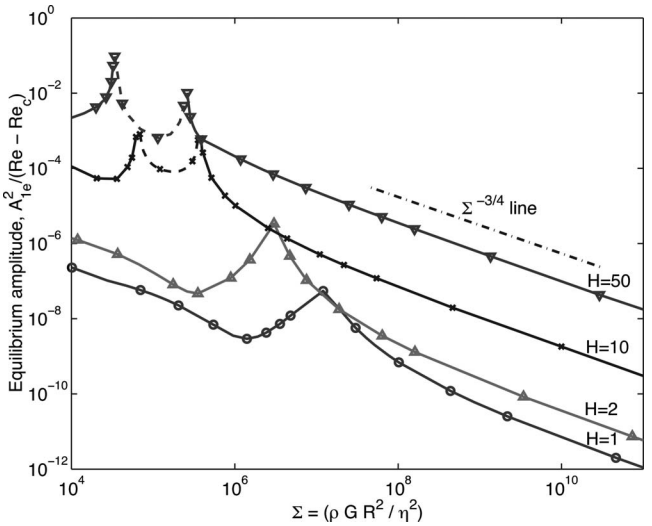

FIG. 13. The equilibrium disturbance amplitude $A_{1e}^2/(\mathrm{Re}-\mathrm{Re}_c)$ as a function of system parameter Σ for different values of H: ○, $H=1$; △, $H=2$; ×, $H=10$; ▽, $H=50$. The broken line is used for the subcritical bifurcation and solid line for the supercritical bifurcation.

all values of H shown in the figure, $s_r^{(1)}$ is negative for high Re wall modes and scales as $\mathrm{Re}^{-1/3}$ in the limit $\mathrm{Re}\gg 1$.

For a given system parameter $\Sigma=\rho G R^2/\eta^2$, the equilibrium amplitude of the bifurcating state can also be represented in the form $A_{1e}^2/(\mathrm{Re}-\mathrm{Re}_c)$. This is obtained from the equilibrium Landau equation expanded in the vicinity of the critical Reynolds number Re_c:

$$0=(\mathrm{Re}-\mathrm{Re}_c)\left.\frac{ds_r^{(0)}}{d\,\mathrm{Re}}\right|_{\Sigma}+A_{1e}^2 s_r^{(1)}+\cdots. \tag{43}$$

Figure 13 shows the variation in $A_{1e}^2/(\mathrm{Re}-\mathrm{Re}_c)$ with the flow independent parameter Σ for different values of H. The critical Reynolds number corresponding to these curves was shown earlier in Figs. 7 and 8. The equilibrium amplitude is found to decrease proportionally to $\Sigma^{-3/4}$ in the limit $\Sigma\gg 1$.

The variation in $s_r^{(1)}$ with solid thickness H is shown in Fig. 14 for $\mathrm{Re}=10^6$. The corresponding critical parameters Γ_c and α_c, about which the Landau constant is evaluated, were shown earlier in Fig. 6. At this Reynolds number, the nature of bifurcation of the wall mode instability is supercritical as $s_r^{(1)}$ is negative for the full range of H shown in the figure. The value of $-s_r^{(1)}$ decreases proportionally to $H^{-3.7}$ for $H\gg 1$, indicating that the stabilizing influence of the nonlinearities diminishes as H increases. The equilibrium amplitude, $A_{1e}^2/(\Gamma-\Gamma_c)$, also plotted in the figure, is found to increase as $H^{2.3}$ for $H\gg 1$. Thus, for $\Gamma>\Gamma_c$, the linearly unstable flow due to infinitesimal amplitude disturbance approaches the supercritically stable state which is $O(A_{1e}^2)$

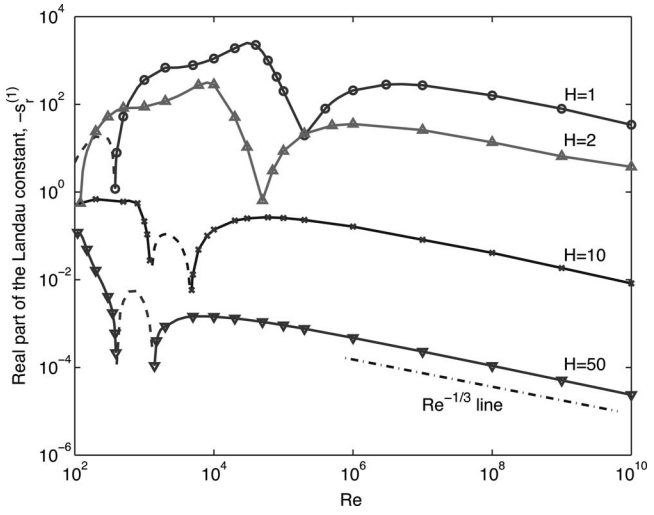

FIG. 12. The real part of the Landau constant $-s_r^{(1)}$ as a function of Reynolds number for different values of H: ○, $H=1$; △, $H=2$; ×, $H=10$; ▽, $H=50$. The respective Γ_c for these curves were shown in Figs. 7 and 8. The broken line is used when $s_r^{(1)}$ is positive and the solid line when $s_r^{(1)}$ is negative.

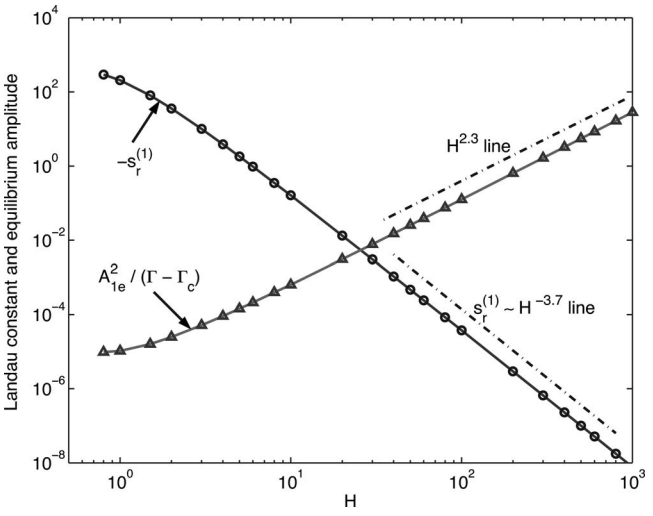

FIG. 14. Variation in the Landau constant $-s_r^{(1)}$ (○) and the equilibrium amplitude $A_{1e}^2/(\Gamma-\Gamma_c)$ (△) with the solid thickness H for $\mathrm{Re}=10^6$. At this Reynolds number, $s_r^{(1)}$ is negative for the entire range of H examined. The dashed-dot lines are the reference lines showing different scaling behaviors.

away from the Couette flow base state and the extent of distortion of the laminar mean flow increases as the elastic solid thickens.

2. Asymptotic analysis

The above discussed results obtained using the numerical technique can be verified with the help of an asymptotic analysis in the limit $\mathrm{Re} \gg 1$. The problems at higher orders leading to the first Landau constant can be solved using asymptotic analysis in the high Reynolds number limit in a manner identical to the linear stability analysis at $k=1$ and $n=1$. Only an overview of the analysis is provided here, and the methodology and the set of governing equations for the asymptotic analysis are provided and briefly discussed in Appendix B.

The wall layer thickness $\delta \equiv \mathrm{Re}^{-1/3}$ provides a small parameter in which all the perturbation quantities are expanded. In amplitude-harmonic expansion (27), we encounter a sequence of problems for eigenfunctions $\tilde{\phi}^{(k,n)}$, where k is the harmonic index and n is the amplitude order. The essence of the asymptotic analysis for the finite amplitude stability is to expand all the eigenfunctions $\tilde{\phi}^{(k,n)}$ in a series in the small parameter δ. Thus, the first few terms in the harmonic-amplitude expansion of a general perturbation,

$$\phi'(x,y,t) = \tilde{\phi}^{(1,1)} E A_1 + [\tilde{\phi}^{(0,2)} + \tilde{\phi}^{(2,2)} E^2] A_1^2 + \tilde{\phi}^{(1,3)} E A_1^3 + \cdots + \text{c.c.}, \tag{44}$$

where $E(x,t) = \exp[i\alpha(x-ct)]$ and c.c. denotes the complex conjugate, becomes

$$\begin{aligned}\phi' = {} & (\tilde{\phi}_0^{(1,1)} + \tilde{\phi}_1^{(1,1)}\delta + \cdots) E A_1 \\ & + [(\tilde{\phi}_0^{(0,2)} + \tilde{\phi}_1^{(0,2)}\delta + \cdots) + (\tilde{\phi}_0^{(2,2)} + \tilde{\phi}_1^{(2,2)}\delta + \cdots) E^2] A_1^2 \\ & + (\tilde{\phi}_0^{(1,3)} + \tilde{\phi}_1^{(1,3)}\delta + \cdots) E A_1^3 + \cdots + \text{c.c.}\end{aligned} \tag{45}$$

Here, the subscripts 0 and 1 represent the quantities leading order in δ and their first correction. Likewise, the Landau equation (28) is written as

$$A_1(\tau)^{-1} d_t A_1(\tau) = (s_{r0}^{(0)} + s_{r1}^{(0)}\delta) + (s_{r0}^{(1)} + s_{r1}^{(1)}\delta) A_1(\tau)^2 + \cdots. \tag{46}$$

The above expansion makes an assumption about the relative order of magnitude of the two small parameters involved in the series, that is, $\delta \gg A_1^2$. The numerical results show that the equilibrium amplitude $A_{1e}^2/(\Gamma - \Gamma_c)$ is proportional to $\mathrm{Re}^{-1/3}$ in the limit $\mathrm{Re} \gg 1$ (refer to Fig. 11). Therefore, in the vicinity of the critical point, such that $\Gamma - \Gamma_c \ll 1$, we have $A_{1e}^2 \ll \delta$. Hence, the asymptotic expansion (46) holds near the critical point for $\mathrm{Re} \gg 1$. Further, the agreement between the numerical and asymptotically calculated Landau constants, to be discussed later in this section, supports the methodology of the asymptotic analysis.

The leading order equations for the (1,3) problem provides $O(1)$ terms in solvability condition (B30) which in turn gives the leading order Landau constant $s_0^{(1)}$ for which nontrivial solutions are admitted. It is found that $s_0^{(1)}$ is always imaginary for all values of solid thickness H considered.

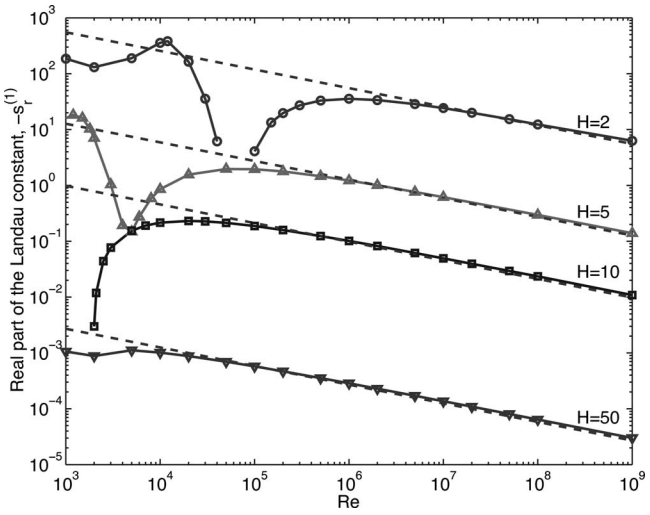

FIG. 15. Comparison of the real part of the Landau constant $-s_r^{(1)}$ obtained from the numerical technique (solid lines with symbols) with that estimated by the asymptotic analysis (broken lines): ○, $H=2$, $\alpha=3$; △, $H=5$, $\alpha=1$; □, $H=10$, $\alpha=0.5$; ▽, $H=50$, $\alpha=0.1$. The broken lines follow the asymptotic solution, $s_r^{(1)} = s_{r1}^{(1)} \mathrm{Re}^{-1/3}$. The numerical results are plotted only when the bifurcation is supercritical ($s_r^{(1)} < 0$).

Since the real part $s_{r0}^{(1)}$ is zero, the leading order solutions do not suggest the nature of nonlinear bifurcation at the critical point. Consequently, the first corrections to the governing equations are solved leading to $O(\delta)$ terms in the solvability condition, which provides the first correction to the Landau constant $s_1^{(1)}$. For all the values of H considered, $s_1^{(1)}$ is found to be a complex number, $s_1^{(1)} = s_{r1}^{(1)} + s_{i1}^{(1)} i$. Thus, the real part of the Landau constant is recovered at $O(\delta)$ and is given by $s_r^{(1)} = s_{r1}^{(1)}\delta$. It should be recalled here that the real part of the Landau constant obtained by numerical computations follows the scaling $s_r^{(1)} \sim \mathrm{Re}^{-1/3}$ (refer to Fig. 12), which is consistent with the results of asymptotic analysis. The quantitative agreement between the numerically and asymptotically computed $s_r^{(1)}$ is shown in Fig. 15. The results from both the methods are found to be in good agreement for $\mathrm{Re} \gg 1$. The agreement is reached at lower Reynolds numbers for the thicker solids. The asymptotic results for the Landau constant $s^{(1)}$ are tabulated in Table II for different values of H and are compared with the numerical solutions. The agreement is observed to improve with an increase in the Reynolds number, as expected.

VI. CONCLUSIONS

The stability of wall modes in shear flow past a flexible surface is analyzed using a combination of asymptotic and numerical methods. The flexible wall is described as an incompressible neo-Hookean elastic solid continuum and the fluid is Newtonian. Both the linear and weakly nonlinear stability analyses are carried out for the high Reynolds number wall mode instability. The critical shear rate Γ_c is found to be close to Γ_c for a linear elastic solid.[23] The bifurcation to the finite amplitude states is examined along the neutral stability curve using the weakly nonlinear stability analysis. The nature of bifurcation depends on the nonlinearities which are of three types. While the fluid governing equations

TABLE II. Comparison of the first Landau constant $s^{(1)}$ obtained from the asymptotic analysis with that evaluated by the numerical technique for different sets of parameters H and α. The asymptotic analysis furnishes the Landau constant in the form $s^{(1)}=s_{i0}^{(1)}+(s_{r1}^{(1)}+s_{i1}^{(1)}i)\mathrm{Re}^{-1/3}$. The real part of the leading order Landau constant $s_{r0}^{(1)}$ is found to be zero.

Re	Asymptotic	Numerical
	$H=5,\ \alpha=1.0$	
	$s_{i0}^{(1)}=-0.544\ 655,\ s_{r1}^{(1)}=-126.878\ 789,\ s_{i1}^{(1)}=-3.022\ 155$	
10^5	$-2.733\ 520-0.479\ 545i$	$-1.947\ 864+0.945\ 570i$
10^7	$-0.588\ 919-0.558\ 683i$	$-0.616\ 241-0.219\ 891i$
10^9	$-0.126\ 878-0.547\ 677i$	$-0.139\ 081-0.482\ 549i$
	$H=10,\ \alpha=0.5$	
	$s_{i0}^{(1)}=-0.068\ 083,\ s_{r1}^{(1)}=-9.822\ 605,\ s_{i1}^{(1)}=-5.214\ 123$	
10^5	$-0.211\ 622-0.180\ 417i$	$-0.187\ 606+0.046\ 145i$
10^7	$-0.045\ 592-0.092\ 284i$	$-0.049\ 296-0.043\ 800i$
10^9	$-0.009\ 823-0.073\ 297i$	$-0.010\ 869-0.062\ 743i$
	$H=50,\ \alpha=0.1$	
	$s_{i0}^{(1)}=-0.000\ 545,\ s_{r1}^{(1)}=-0.027\ 027,\ s_{i1}^{(1)}=-0.012\ 143$	
10^5	$(-5.822\ 790-8.065\ 795i)\times10^{-4}$	$(-5.745\ 253-2.683\ 160i)\times10^{-4}$
10^7	$(-1.254\ 482-6.013\ 242i)\times10^{-4}$	$(-1.367\ 060-4.804\ 367i)\times10^{-4}$
10^9	$(-0.270\ 270-5.571\ 033i)\times10^{-4}$	$(-0.300\ 701-5.306\ 324i)\times10^{-4}$

have convective nonlinearities at finite Reynolds numbers, the solid equations admit nonlinear terms due to the finite strain neo-Hookean model. Moreover, the matching conditions at the deformed fluid-solid interface, which are expressed in Taylor series expansions about the unperturbed interface, result in nonlinearities. In the weakly nonlinear stability analysis, the first Landau constant $s^{(1)}$ is calculated for a range of Reynolds numbers and solid thickness H.

In the Stokes flow limit $\mathrm{Re}\ll1$, $s_r^{(1)}$ is positive, indicating subcritical bifurcation for the viscous instability. In the intermediate Reynolds number, $s_r^{(1)}$ changes its sign three times before settling to a negative sign for $\mathrm{Re}\gg1$. Hence, the bifurcation is supercritical for the wall mode instability at high Reynolds numbers. In the limit $\mathrm{Re}\gg1$, the results obtained using the numerical technique are verified using an asymptotic analysis. The high Reynolds number asymptotics suggests that the real part of the Landau constant is negative and it scales as $\mathrm{Re}^{-1/3}$ in the limit $\mathrm{Re}\gg1$, in agreement with numerical results. Using the Landau constant, the equilibrium amplitude (A_{1e}) is derived in the neighborhood of the critical point $\Gamma=\Gamma_c$. Since $s_r^{(1)}$ is negative for the wall mode instability, the unstable flow at $\Gamma>\Gamma_c$ leads to a new stationary state which deviates by $O(A_{1e}^2)$ from the laminar flow base state. The equilibrium amplitude, in the form $A_{1e}^2/(\Gamma-\Gamma_c)$, is found to be proportional to $\mathrm{Re}^{-1/3}$ in the limit $\mathrm{Re}\gg1$. The effect of solid thickness H on the weakly nonlinear stability shows that the equilibrium amplitude $A_{1e}^2/(\Gamma-\Gamma_c)$ increases with the solid thickness and is proportional to $H^{2.3}$ for $H\gg1$, indicating the destabilizing influence of solid thickness on the wall mode instability.

There are two important results of the present analysis. The first is that there is not much difference between the stability results for the linear and the neo-Hookean constitutive relations for the solid. This indicates that the linear elastic model is adequate for capturing both the instability as well as the secondary flow that develops after instability. This is in contrast to the limit of low Reynolds numbers, where it has been found that the results are quantitatively different for the linear and the neo-Hookean constitutive relations.[25] This indicates that the high Reynolds number instability is less influenced by the details of the solid constitutive relations than the low Reynolds number instability. In addition, we have shown that the asymptotic analysis used to identify the scalings in the linear stability problem can be used to obtain scalings for the equilibrium amplitude in the nonlinear analysis as well.

The second important result is that the wall mode instability in the flow past a flexible surface is a rare example of a shear flow instability where the bifurcation is supercritical. The Tollmien–Schlichting instability in the flow through a rigid channel is subcritical, while the flow through a pipe does not become unstable in the linear stability analysis. The supercritical nature of the bifurcation could be of importance in two respects. First, if the transition Reynolds number for the wall mode instability is lower than that for the transition to turbulence in a rigid channel, the flow after transition would have very different characteristics from a turbulent flow. The transition to turbulence would now depend on the instability of the stationary state that is generated due to the wall mode instability, and the Reynolds number for this could be different from that for a laminar flow past a rigid surface. In addition, the increase in drag would be continuous when the wall mode instability sets in because the bifurcation is supercritical. This is in contrast to the discontinuous increase in drag which is a consequence of the transition to turbulence. Second, even if the transition to turbulence takes place at a Reynolds number lower than the critical Reynolds number for the wall mode instability, the wall mode instability could still influence the turbulent flow because it is confined to a thin layer at the wall in the limit of high Reynolds numbers. In this case, the near wall vortical structures that form, and their bursting, could be affected by the secondary flow generated by the wall mode instability. A question of importance is whether this would increase or reduce the drag in the turbulent flow.

APPENDIX A: SOLUTION PROCEDURE

1. The (1,1) problem

The disturbance with harmonic index $k=1$ and amplitude order $n=1$ is the fundamental mode and the problem at this order corresponds to the linear stability problem. The dimensionless fluid governing equations at this order are

$$i\alpha\tilde{v}_x^{(1,1)}+d_y\tilde{v}_y^{(1,1)}=0, \tag{A1}$$

$$i\alpha(\Gamma y-c)\tilde{v}_x^{(1,1)}+\Gamma\tilde{v}_y^{(1,1)}=-i\alpha\tilde{p}_f^{(1,1)}+\frac{\Gamma}{\mathrm{Re}}(d_y^2-\alpha^2)\tilde{v}_x^{(1,1)}, \tag{A2}$$

$$i\alpha(\Gamma y - c)\tilde{v}_y^{(1,1)} = -d_y\tilde{p}_f^{(1,1)} + \frac{\Gamma}{\mathrm{Re}}(d_y^2 - \alpha^2)\tilde{v}_y^{(1,1)}, \tag{A3}$$

where $d_y = d/d_y$, $\Gamma = \sqrt{\rho V^2/G}$ is the dimensionless top plate velocity, and Reynolds number $\mathrm{Re} = \rho VR/\eta$. The mass and momentum conservation equations for the neo-Hookean solid medium are

$$i\alpha\tilde{u}_x^{(1,1)} + d_y\tilde{u}_y^{(1,1)} + i\alpha\frac{\Gamma^2}{\mathrm{Re}}\tilde{u}_y^{(1,1)} = 0,$$

$$-\alpha^2c^2\tilde{u}_x^{(1,1)} - \alpha^2c^2\frac{\Gamma^2}{\mathrm{Re}}\tilde{u}_y^{(1,1)} = -i\alpha\tilde{p}_g^{(1,1)} + \left[(d_y^2 - \alpha^2)\tilde{u}_x^{(1,1)} - i\alpha\frac{\Gamma^2}{\mathrm{Re}}d_y\tilde{u}_x^{(1,1)} + \alpha^2\frac{\Gamma^2}{\mathrm{Re}}\tilde{u}_y^{(1,1)}\right], \tag{A4}$$

$$-\alpha^2c^2\tilde{u}_y^{(1,1)} = -d_y\tilde{p}_g^{(1,1)} + \left[(d_y^2 - \alpha^2)\tilde{u}_y^{(1,1)} - i\alpha\frac{\Gamma^2}{\mathrm{Re}}d_y\tilde{u}_y^{(1,1)} + \alpha^2\frac{\Gamma^2}{\mathrm{Re}}\tilde{u}_x^{(1,1)} - 2\frac{\Gamma^2}{\mathrm{Re}}d_y^2\tilde{u}_x^{(1,1)}\right],$$

where c is the complex-valued disturbance wavespeed, such that the linear growth rate $s^{(0)} = -i\alpha c$. The overall solid governing equation, upon eliminating the pressure, is

$$\left[d_y^4 + 2i\alpha\frac{\Gamma^2}{\mathrm{Re}}d_y^3 - \alpha^2\left(2 + \frac{\Gamma^4}{\mathrm{Re}^2}\right)d_y^2 - 2i\alpha^3\frac{\Gamma^2}{\mathrm{Re}}d_y + \alpha^4\left(1 + \frac{\Gamma^4}{\mathrm{Re}^2}\right)\right]\tilde{u}_y^{(1,1)} + \alpha^2c^2(d_y^2 - \alpha^2)\tilde{u}_y^{(1,1)} = 0. \tag{A5}$$

The boundary conditions for this problem include $\tilde{v}_y^{(1,1)} = \tilde{v}_x^{(1,1)} = 0$ at $y = 1$ and $\tilde{u}_y^{(1,1)} = \tilde{u}_x^{(1,1)} = 0$ at $y = -H$. At the perturbed fluid-solid interface, the Taylor expansion of the interfacial continuity conditions results in the following conditions to be enforced at $y = 0$:

$$\tilde{v}_y^{(1,1)} = -i\alpha c\tilde{u}_y^{(1,1)}, \tag{A6}$$

$$\tilde{v}_x^{(1,1)} + \Gamma\tilde{u}_y^{(1,1)} = -i\alpha c\tilde{u}_x^{(1,1)} - i\alpha c\frac{\Gamma^2}{\mathrm{Re}}\tilde{u}_y^{(1,1)}, \tag{A7}$$

$$\frac{\Gamma}{\mathrm{Re}}(d_y\tilde{v}_x^{(1,1)} + i\alpha\tilde{v}_y^{(1,1)}) = \left(d_y\tilde{u}_x^{(1,1)} + i\alpha\tilde{u}_y^{(1,1)} - i\alpha\frac{\Gamma^2}{\mathrm{Re}}\tilde{u}_x^{(1,1)}\right) - i\alpha\frac{\Gamma^4}{\mathrm{Re}^2}\tilde{u}_y^{(1,1)}, \tag{A8}$$

$$-\tilde{p}_f^{(1,1)} + 2\frac{\Gamma}{\mathrm{Re}}d_y\tilde{v}_y^{(1,1)} = -\tilde{p}_g^{(1,1)} + 2\left(d_y\tilde{u}_y^{(1,1)} - \frac{\Gamma^2}{\mathrm{Re}}d_y\tilde{u}_x^{(1,1)}\right). \tag{A9}$$

Equation (A6) is the normal-velocity continuity condition at the fluid-solid interface. Equation (A7) gives the tangential-velocity continuity condition, wherein the second term on the left-hand side is due to a jump in mean flow shear rate across the interface. The right-hand side is the expression for the Eulerian velocity field in the solid which contains a base-fluctuation coupling term due to the finite displacement gradient (Γ^2/Re) in the base state. The tangential-stress continuity is given by Eq. (A8). Here, the last term on the right-hand side is due to a jump in normal-stress difference across the interface. As shown in Sec. II, the neo-Hookean solid exhibits nonzero first normal-stress difference, $\bar{\sigma}_{xx} - \bar{\sigma}_{yy} = \Gamma^4/\mathrm{Re}^2$, for the plane shear flow. This normal-stress difference contributes to the perturbation tangential-stress due to the nonflat interface. Equation (A9) is the normal-stress continuity condition. The fluid-solid interfacial tension is ignored. Importantly, all the terms containing Γ^2/Re on the right-hand side of the above conditions are due to the finite strain deformations permissible in the neo-Hookean model. These terms are absent for the linear viscoelastic gel model.[23]

First, the eigenvalue c is obtained using the shooting technique. The numerical technique is discussed in detail in Ref. 15 and has been used previously.[20] The transition value of fluid shear rate Γ for the onset of instability is obtained by setting the imaginary part of the wavespeed c_i to zero. For the weakly nonlinear stability analysis, the eigenfunctions corresponding to the most unstable wall mode are obtained using the Chebyshev collocation method. An additional "normalization" condition is required, which we specify here as $\tilde{u}_x^{(1,1)}|_{y=0} = 1 + i$. Thus, the eigenfunctions and all the subsequent results including the value of the Landau constant $s^{(1)}$ are specific to the given normalization condition.

2. The (0,2) and (2,2) problems

The problem with harmonic index $k = 0$ and amplitude exponent $n = 2$ represents the correction to the mean flow due to nonlinear interactions and the one at order $k = 2$ and $n = 2$ is the first harmonic of the fundamental mode. The governing equations for the (0,2) and (2,2) problems are similar to the expressions for the (1,1) problem with wavenumber α being replaced with 0 and 2α, respectively. In addition, the inhomogeneous terms containing the eigenfunctions of the (1,1) problem appear in the right-hand side of the governing equations for the fluid [Eqs. (A2) and (A3)] and the solid dynamics [Eqs. (A4) and (A5)]. The inhomogeneities arise due to the nonlinearities present in these equations. The inhomogeneous equations are solved using the no-slip conditions at the top and bottom plates and the matching conditions at the perturbed interface, which are expanded about the flat interface. As the Taylor expansion results in nonlinear terms, the interface conditions also carry the inhomogeneities in terms of the eigenfunctions of the (1,1) problem.

3. The (1,3) problem

The problem at order $k = 1$ and $n = 3$ is $O(A_1^2)$ correction to the fundamental mode. It features the variation in amplitude with slow time scale $A_1(\tau)$. Thus, the Landau equation (28) is recovered at this order. The fluid governing equations are

$$i\alpha\tilde{v}_x^{(1,3)} + d_y\tilde{v}_y^{(1,3)} = 0, \tag{A10}$$

$$-i\alpha(\Gamma y - c)\tilde{v}_x^{(1,3)} - \Gamma\tilde{v}_y^{(1,3)} - i\alpha\tilde{p}_f^{(1,3)} + (d_y^2 - \alpha^2)\tilde{v}_x^{(1,3)} = \mathcal{I}_x^{(1,3)}, \tag{A11}$$

$$-i\alpha(\Gamma y - c)\tilde{v}_y^{(1,3)} - d_y\tilde{p}_f^{(1,3)} + (d_y^2 - \alpha^2)\tilde{v}_y^{(1,3)} = \mathcal{I}_y^{(1,3)}. \tag{A12}$$

The governing equations for the neo-Hookean solid at this order are

$$i\alpha\tilde{u}_x^{(1,3)} + d_y\tilde{u}_y^{(1,3)} + i\alpha\frac{\Gamma^2}{\mathrm{Re}}\tilde{u}_y^{(1,3)} = \mathcal{J}_c^{(1,3)}, \tag{A13}$$

$$\left[d_y^4 + 2i\alpha\frac{\Gamma^2}{\mathrm{Re}}d_y^3 - \alpha^2\left(2 + \frac{\Gamma^4}{\mathrm{Re}^2}\right)d_y^2 - 2i\alpha^3\frac{\Gamma^2}{\mathrm{Re}}d_y + \alpha^4\left(1 + \frac{\Gamma^4}{\mathrm{Re}^2}\right)\right]\tilde{u}_y^{(1,3)} + \alpha^2c^2(d_y^2 - \alpha^2)\tilde{u}_y^{(1,3)} = \mathcal{J}^{(1,3)}. \tag{A14}$$

In the above expressions the left-hand sides indicate the inhomogeneous terms arising due to various nonlinear interactions of the previously solved problems such as the interaction of the fundamental mode (1,1) with (0,2) eigenfunctions and the interaction of the first harmonic mode (2,2) with the conjugate of the fundamental mode $(-1,1)$. The fluid inhomogeneities $\mathcal{I}_x^{(1,3)}$ and $\mathcal{I}_y^{(1,3)}$ and the solid inhomogeneity $\mathcal{J}^{(1,3)}$ contain the first Landau constant $s^{(1)}$.

In addition to the no-slip conditions at the top and bottom walls, the following interface conditions are required to be satisfied at $y=0$:

$$\tilde{v}_y^{(1,3)} + i\alpha c\tilde{u}_y^{(1,3)} = \gamma_1^{(1,3)}, \tag{A15}$$

$$\tilde{v}_x^{(1,3)} + \Gamma\tilde{u}_y^{(1,3)} + i\alpha c\tilde{u}_x^{(1,3)} + i\alpha c\frac{\Gamma^2}{\mathrm{Re}}\tilde{u}_y^{(1,3)} = \gamma_2^{(1,3)}, \tag{A16}$$

$$\frac{\Gamma}{\mathrm{Re}}(d_y\tilde{v}_x^{(1,3)} + i\alpha\tilde{v}_y^{(1,3)}) - \left(d_y\tilde{u}_x^{(1,3)} + i\alpha\tilde{u}_y^{(1,3)} - i\alpha\frac{\Gamma^2}{\mathrm{Re}}\tilde{u}_x^{(1,3)}\right) + i\alpha\frac{\Gamma^4}{\mathrm{Re}^2}\tilde{u}_y^{(1,3)} = \gamma_3^{(1,3)}, \tag{A17}$$

$$-\tilde{p}_f^{(1,3)} + 2\frac{\Gamma}{\mathrm{Re}}d_y\tilde{v}_y^{(1,3)} + \tilde{p}_g^{(1,3)} - 2\left(d_y\tilde{u}_y^{(1,3)} - \frac{\Gamma^2}{\mathrm{Re}}d_y\tilde{u}_x^{(1,3)}\right) = \gamma_4^{(1,3)}. \tag{A18}$$

Here, the inhomogeneities $\gamma_1^{(1,3)}$ and $\gamma_2^{(1,3)}$ contain the variation in $A(\tau)$ with τ as the material time derivative of displacement is taken to obtain the solid velocity.

The governing equations and boundary conditions discretized using the Chebyshev collocation scheme are expressed schematically as

$$\mathbf{M}\boldsymbol{\phi} = \boldsymbol{\gamma}^{(1,3)}, \tag{A19}$$

where ϕ denotes the (1,3) eigenfunctions at collocation points. Since the left-hand sides of the fluid and solid governing equations as well as the interface boundary conditions are similar to the ones encountered in the (1,1) problem, the matrix $\mathbf{M}$ for the present problem is identical to that for the linear problem $(k=1, n=1)$. From the linear stability analysis, $\mathbf{M}$ is known to be singular. Therefore, the inhomogeneous (1,3) problem does not exhibit a unique solution and the Fredholm solvability condition should be satisfied for the (1,3) problem to have nontrivial solutions. In order to formulate the solvability criterion, we need the solution of the homogeneous adjoint problem. The adjoint problem is constructed by defining the inner product of two vectors $\boldsymbol{\phi}$ and $\boldsymbol{\psi}$ as

$$\langle\boldsymbol{\phi},\boldsymbol{\psi}\rangle = \sum_i \boldsymbol{\phi}_i^\dagger\psi_i, \tag{A20}$$

where $\phi_i^\dagger$ is the complex conjugate of ϕ_i. The homogeneous adjoint problem of original problem (A19) is written as

$$\mathbf{M}^*\boldsymbol{\psi} = \mathbf{0}, \tag{A21}$$

where $M_{ij}^* = M_{ji}^\dagger$ is the adjoint of matrix $\mathbf{M}$ and $\boldsymbol{\psi}$ is the nontrivial solution for the homogeneous adjoint problem which can be obtained using any additional condition on vector $\boldsymbol{\psi}$. The Fredholm solvability criterion is to make $\boldsymbol{\psi}$ orthogonal to the inhomogeneity vector $\boldsymbol{\gamma}^{(1,3)}$:

$$\langle\boldsymbol{\psi},\boldsymbol{\gamma}^{(1,3)}\rangle = 0. \tag{A22}$$

On substituting the solution of the adjoint function ψ, the Landau equation is recovered from the above solvability condition as, after taking the real part,

$$A_1(\tau)^{-1}d_tA_1(\tau) = s_r^{(0)} + A_1(\tau)^2s_r^{(1)} + \cdots, \tag{A23}$$

where $s_r^{(1)}$ is the real part of the first Landau constant. The sign of $s_r^{(1)}$ determines the nature of the bifurcation of the linear instability in the plane with a finite amplitude. If $s_r^{(1)}$ is positive the instability is subcritical, whereas if $s_r^{(1)}$ is negative the instability is of a supercritical nature.

APPENDIX B: ASYMPTOTIC ANALYSIS

In this appendix, the asymptotic analysis to calculate the first Landau constant $s^{(1)}$ is discussed briefly. The fluid domain is split into the wall layer adjacent to the interface and the inviscid outer layer. Within the wall layer with thickness $\delta \equiv \mathrm{Re}^{-1/3}$, the ordinate is scaled as $y = y_0\delta$ and the fluid governing equations in the wall layer are written in terms of "inner" coordinate y_0. For a general problem at order (k,n), the fluid velocity components in the wall layer are expanded as

$$\tilde{v}_{w,x}^{(k,n)}(y_0) = (\tilde{v}_{w,x_0}^{(k,n)} + \tilde{v}_{w,x_1}^{(k,n)}\delta + \cdots), \tag{B1}$$

$$\tilde{v}_{w,y}^{(k,n)}(y_0) = \delta(\tilde{v}_{w,y_0}^{(k,n)} + \tilde{v}_{w,y_1}^{(k,n)}\delta + \cdots). \tag{B2}$$

The velocity and pressure in the outer inviscid region need to be expanded in the following asymptotic series in order to achieve a balance in the normal-stress continuity condition at the interface:

$$\tilde{v}_{o,x}^{(k,n)}(y) = \delta(\tilde{v}_{o,x_0}^{(k,n)} + \tilde{v}_{o,x_1}^{(k,n)}\delta + \cdots), \tag{B3}$$

$$\tilde{v}_{o,y}^{(k,n)}(y) = \delta(\tilde{v}_{o,y_0}^{(k,n)} + \tilde{v}_{o,y_1}^{(k,n)}\delta + \cdots), \tag{B4}$$

$$\tilde{p}_{o,f}^{(k,n)}(y) = (\tilde{p}_{o,f_0}^{(k,n)} + \tilde{p}_{o,f_1}^{(k,n)}\delta + \cdots). \tag{B5}$$

The displacement field and the pressure in the elastic solid are expanded as

$$\tilde{u}_x^{(k,n)}(y) = (\tilde{u}_{x_0}^{(k,n)} + \tilde{u}_{x_1}^{(k,n)}\delta + \cdots), \tag{B6}$$

$$\tilde{u}_y^{(k,n)}(y) = (\tilde{u}_{y_0}^{(k,n)} + \tilde{u}_{y_1}^{(k,n)}\delta + \cdots), \tag{B7}$$

$$\tilde{p}_g^{(k,n)}(y) = (\tilde{p}_{g_0}^{(k,n)} + \tilde{p}_{g_1}^{(k,n)}\delta + \cdots). \tag{B8}$$

The disturbance wavespeed is written as $c=c_0+c_1\delta+\cdots$ and the fluid shear rate is scaled with the Reynolds number as $\Gamma=\Gamma_0/\delta$, where Γ_0 is $O(1)$ parameter. The leading order linear growth rate is $s_0^{(0)}=-i\alpha c_0$ and its first correction is $s_1^{(0)}=-i\alpha c_1$. The above expansions are substituted in the governing equations for the (k,n) problem and the terms leading order in δ and their next correction are extracted as the governing equations at respective orders.

For the (1,1) problem, the leading order mass and momentum conservation equations for the wall layer in the fluid domain are

$$i\alpha\tilde{v}_{w,x_0}^{(1,1)} + d_{y_0}\tilde{v}_{w,y_0}^{(1,1)} = 0, \tag{B9}$$

$$\left[d_{y_0}^2 - i\alpha\left(y_0 - \frac{c_0}{\Gamma_0}\right)\right]d_{y_0}\tilde{v}_{w,x_0}^{(1,1)} = 0. \tag{B10}$$

The above momentum balance equation possesses the Airy functions $\mathrm{Ai}(z)$ and $\mathrm{Bi}(z)$ as solutions, where the variable z is defined as $z=(i\alpha)^{1/3}(y_0-c_0/\Gamma_0)$. Of these, the solution $\mathrm{Bi}(z)$ is discarded as it diverges in the limit $y_0\to\infty$.[22] In the outer inviscid zone, the leading order fluid governing equations are

$$i\alpha\tilde{v}_{o,x_0}^{(1,1)} + d_y\tilde{v}_{o,y_0}^{(1,1)} = 0, \tag{B11}$$

$$(d_y^2 - \alpha^2)\tilde{v}_{o,y_0}^{(1,1)} = 0, \tag{B12}$$

$$\tilde{p}_{o,f_0}^{(1,1)} = -\Gamma_0 y\tilde{v}_{o,x_0}^{(1,1)} - \Gamma_0\tilde{v}_{o,y_0}^{(1,1)}/(i\alpha). \tag{B13}$$

An order δ correction to the outer layer governing equation yields

$$i\alpha\tilde{v}_{o,x_1}^{(1,1)} + d_y\tilde{v}_{o,y_1}^{(1,1)} = 0, \tag{B14}$$

$$(d_y^2 - \alpha^2)\tilde{v}_{o,y_1}^{(1,1)} = 0, \tag{B15}$$

$$\tilde{p}_{o,f_1}^{(1,1)} = -\Gamma_0 y\tilde{v}_{o,x_1}^{(1,1)} - \Gamma_0\tilde{v}_{o,y_1}^{(1,1)}/(i\alpha) + c_0\tilde{v}_{o,x_0}^{(1,1)}. \tag{B16}$$

The leading order governing equations in the neo-Hookean elastic solid are

$$i\alpha\tilde{u}_{x_0}^{(1,1)} + d_y\tilde{u}_{y_0}^{(1,1)} = 0, \tag{B17}$$

$$(d_y^2 - \alpha^2)^2\tilde{u}_{y_0}^{(1,1)} + \alpha^2 c_0^2(d_y^2 - \alpha^2)\tilde{u}_{y_0}^{(1,1)} = 0, \tag{B18}$$

$$\tilde{p}_{g_0}^{(1,1)} = \frac{1}{i\alpha}[(d_y^2 - \alpha^2)\tilde{u}_{x_0}^{(1,1)} + \alpha^2 c_0^2\tilde{u}_{x_0}^{(1,1)}]. \tag{B19}$$

As the finite strain deformation terms specific to the neo-Hookean model are of the magnitude $O(\delta)$, the solid equations at the leading order are the same as that for the linearly elastic solid. The governing equations for the first correction to the displacements are

$$i\alpha\tilde{u}_{x_1}^{(1,1)} + d_y\tilde{u}_{y_1}^{(1,1)} + i\alpha\Gamma_0^2\tilde{u}_{y_0}^{(1,1)} = 0, \tag{B20}$$

$$(d_y^2 - \alpha^2)^2\tilde{u}_{y_1}^{(1,1)} + \alpha^2 c_0^2(d_y^2 - \alpha^2)\tilde{u}_{y_1}^{(1,1)} + 2\alpha^2 c_0 c_1(d_y^2 - \alpha^2)\tilde{u}_{y_0}^{(1,1)} + (2i\alpha\Gamma_0^2 d_y^3 - 2i\alpha^3\Gamma_0^2 d_y)\tilde{u}_{y_0}^{(1,1)} = 0, \tag{B21}$$

$$\tilde{p}_{g_1}^{(1,1)} = \frac{1}{i\alpha}[(d_y^2 - \alpha^2)\tilde{u}_{x_1}^{(1,1)} + \alpha^2\Gamma_0^2\tilde{u}_{y_0}^{(1,1)} - i\alpha\Gamma_0^2 d_y\tilde{u}_{x_0}^{(1,1)} + \alpha^2 c_0^2\tilde{u}_{x_0}^{(1,1)} + 2\alpha^2 c_0 c_1\tilde{u}_{x_0}^{(1,1)} + \alpha^2 c_0^2\Gamma_0^2\tilde{u}_{y_0}^{(1,1)}]. \tag{B22}$$

The above set of governing equations is solved analytically by imposing the no-slip boundary conditions at the top and bottom plates. In addition, the following conditions at the fluid-solid interface need to be enforced at $y=y_0=0$:

$$i\alpha c_0\tilde{u}_{y_0}^{(1,1)} + \delta[\tilde{v}_{o,y_0}^{(1,1)} + \tilde{v}_{w,y_0}^{(1,1)} + i\alpha c_0\tilde{u}_{y_1}^{(1,1)} + i\alpha c_1\tilde{u}_{y_0}^{(1,1)}] = 0, \tag{B23}$$

$$\frac{\Gamma_0}{\delta}\tilde{u}_{y_0}^{(1,1)} + [\tilde{v}_{w,x_0}^{(1,1)} + \Gamma_0\tilde{u}_{y_1}^{(1,1)} + i\alpha c_0\tilde{u}_{x_0}^{(1,1)}] = 0, \tag{B24}$$

$$-d_y\tilde{u}_{x_0}^{(1,1)} + \delta[\Gamma_0 d_{y_0}\tilde{v}_{w,x_0}^{(1,1)} - (d_y\tilde{u}_{x_1}^{(1,1)} + i\alpha\tilde{u}_{y_1}^{(1,1)} - i\alpha\Gamma_0^2\tilde{u}_{x_0}^{(1,1)})] = 0, \tag{B25}$$

$$-\tilde{p}_{o,f_0}^{(1,1)} + \tilde{p}_{g_0}^{(1,1)} - 2d_y\tilde{u}_{y_0}^{(1,1)} + \delta[-\tilde{p}_{o,f_1}^{(1,1)} + \tilde{p}_{g_1}^{(1,1)} - 2d_y\tilde{u}_{y_1}^{(1,1)} + 2\Gamma_0^2 d_y\tilde{u}_{x_0}^{(1,1)}] = 0. \tag{B26}$$

Here, the interface conditions are expanded as the leading order and the first correction terms. Substituting the analytical solutions, the above expressions result in a matrix problem of the form

$$\mathbf{MC} = \mathbf{0}, \tag{B27}$$

where $\mathbf{C}$ is the vector of constants. The characteristic equation $\mathrm{Det}[\mathbf{M}]=0$ is expanded in small parameter δ. The leading order expression yields the eigenvalue c_0, and the first correction yields an expression of c_1. The resultant c_0 and c_1 and the transition parameter Γ_0 are mentioned and discussed in Sec. V A. Next, the fluid and solid eigenfunctions for the (1,1) problem are obtained by solving matrix problem (B27) using the additional normalization condition $\tilde{u}_{x_0}^{(1,1)}|_{y=0}=1+i$.

For the (1,3) problem at amplitude order A_{1e}^3, the governing equations are similar to the equations for the (1,1) problem except that the wall layer equation for the fluid and solid equations contain the inhomogeneities on the right-hand sides. The Landau constant $s^{(1)}$ appears as one of the

inhomogeneous terms. We write the Landau constant in an asymptotic series $s^{(1)}=s_0^{(1)}+\delta s_1^{(1)}+\cdots$. Substituting the analytical solutions in the interface conditions results in the matrix problem

$$\mathbf{MC}=\mathbf{b}, \tag{B28}$$

where **C** is the vector of constants and the vector on inhomogeneities **b** contains the leading order and the first correction Landau constants, $s_0^{(1)}$ and $s_1^{(1)}$. As matrix **M** is similar to the one that occurred in the (1,1) problem, it is known to be singular. Hence, for the nontrivial solutions to exist, the Fredholm solvability condition needs to be satisfied, which requires the solution of the homogeneous adjoint problem

$$\mathbf{M}^*\boldsymbol{\psi}=\mathbf{0}, \tag{B29}$$

where $M_{ij}^*=M_{ji}^\dagger$ is the adjoint of matrix **M**. The solution $\boldsymbol{\psi}$ is obtained by using any additional condition on the vector $\boldsymbol{\psi}$. The solvability condition requires the inhomogeneity vector **b** to be orthogonal to $\boldsymbol{\psi}$, that is,

$$\langle \mathbf{b}, \boldsymbol{\psi} \rangle = 0. \tag{B30}$$

This condition contains leading order terms of $O(1)$ and the first correction terms of $O(\delta)$. The leading order part gives the leading order Landau constant $s_0^{(1)}$ and the first correction part provides the $O(\delta)$ correction to Landau constant $s_1^{(1)}$.

[1] G. M. Corcos and J. R. Sellars, "On the stability of fully developed pipe flow," J. Fluid Mech. **5**, 97 (1959).
[2] A. E. Gill, "On the behavior of small disturbances to Poiseuille flow in a circular pipe," J. Fluid Mech. **21**, 145 (1965).
[3] A. Davey and P. G. Drazin, "The stability of Poiseuille flow in a pipe," J. Fluid Mech. **36**, 209 (1969).
[4] F. Waleffe, "On a self-sustaining process in shear flows," Phys. Fluids **9**, 883 (1997).
[5] F. Waleffe, "Three-dimensional coherent states in plane shear flows," Phys. Rev. Lett. **81**, 4140 (1998).
[6] W. Schoppa and F. Hussain, "Coherent structure generation in near-wall turbulence," J. Fluid Mech. **453**, 57 (2002).
[7] T. Itano and S. Toh, "The dynamics of bursting process in wall turbulence," J. Phys. Soc. Jpn. **70**, 703 (2001).
[8] M. O. Kramer, "Boundary-layer stabilization by distributed damping," J. Aeronaut. Sci. **24**, 458 (1957).
[9] T. B. Benjamin, "Effect of a flexible surface on boundary layer stability," J. Fluid Mech. **9**, 513 (1960).
[10] T. B. Benjamin, "The threefold classification for unstable disturbances in flexible surfaces bounding inviscid flows," J. Fluid Mech. **16**, 436 (1963).
[11] P. W. Carpenter, A. D. Lucey, and C. Davies, "Progress on the use of compliant walls for laminar flow control," J. Aircr. **38**, 504 (2001).
[12] P. Krindel and A. Silberberg, "Flow through gel-walled tubes," J. Colloid Interface Sci. **71**, 39 (1979).
[13] V. Kumaran, G. H. Fredrickson, and P. Pincus, "Flow induced instability of the interface between a fluid and a gel at low Reynolds number," J. Phys. II (France) **4**, 893 (1994).
[14] V. Kumaran, "Stability of the viscous flow of a fluid through a flexible tube," J. Fluid Mech. **294**, 259 (1995).
[15] L. Srivatsan and V. Kumaran, "Flow induced instability of the interface between a fluid and a gel," J. Phys. II (France) **7**, 947 (1997).
[16] V. Kumaran, "Stability of fluid flow through a flexible tube at intermediate Reynolds number," J. Fluid Mech. **357**, 123 (1998).
[17] V. Kumaran and R. Muralikrishnan, "Spontaneous growth of fluctuations in the viscous flow of a fluid past a soft interface," Phys. Rev. Lett. **84**, 3310 (2000).
[18] R. Muralikrishnan and V. Kumaran, "Experimental study of the instability of the viscous flow past a flexible surface," Phys. Fluids **14**, 775 (2002).
[19] M. D. Eggert and S. Kumar, "Observations of instability, hysteresis, and oscillation in low-Reynolds number flow past polymer gels," J. Colloid Interface Sci. **278**, 234 (2004).
[20] V. Kumaran, "Stability of wall modes in a flexible tube," J. Fluid Mech. **362**, 1 (1998).
[21] V. Kumaran, "Asymptotic analysis of wall modes in a flexible tube," Eur. Phys. J. B **4**, 519 (1998).
[22] V. Shankar and V. Kumaran, "Asymptotic analysis of wall modes in a flexible tube revisited," Eur. Phys. J. B **19**, 607 (2001).
[23] V. Shankar and V. Kumaran, "Stability of wall modes in fluid flow past a flexible surface," Phys. Fluids **14**, 2324 (2002).
[24] L. E. Malvern, *Introduction to the Mechanics of a Continuous Medium* (Prentice-Hall, Englewood Cliffs, NJ, 1969).
[25] V. Gkanis and S. Kumar, "Instability of creeping Couette flow past a neo-Hookean solid," Phys. Fluids **15**, 2864 (2003).
[26] V. Gkanis and S. Kumar, "Stability of pressure-driven creeping flows in channels lined with a nonlinear elastic solid," J. Fluid Mech. **524**, 357 (2005).
[27] V. Gkanis and S. Kumar, "Instability of gravity-driven free-surface flow past a deformable elastic solid," Phys. Fluids **18**, 044103 (2006).
[28] S. A. Roberts and S. Kumar, "Stability of creeping Couette flow of a power-law fluid past a deformable solid," J. Non-Newtonian Fluid Mech. **139**, 93 (2006).
[29] J. Adepu and V. Shankar, "Suppression or enhancement of interfacial instability in two-layer plane Couette flow of FENE-P fluids past a deformable solid layer," J. Non-Newtonian Fluid Mech. **141**, 43 (2007).
[30] J. M. Rotenberry and P. G. Saffman, "Effect of compliant boundaries on weakly nonlinear shear waves in channel flow," SIAM J. Appl. Math. **50**, 361 (1990).
[31] J. T. Stuart, "On the non-linear mechanics of wave disturbances in stable and unstable parallel flows. Part I. The basic behavior in plane Poiseuille flow," J. Fluid Mech. **9**, 353 (1960).
[32] J. Watson, "On the non-linear mechanics of wave disturbances in stable and unstable parallel flows. Part II. The development of a solution for plane Poiseuille and for plane Couette flow," J. Fluid Mech. **9**, 371 (1960).
[33] V. Shankar and V. Kumaran, "Weakly nonlinear stability of viscous flow past a flexible surface," J. Fluid Mech. **434**, 337 (2001).